School of Science

Van der Waals interactions in density-functional theory: implementation and applications

Andris Guļāns

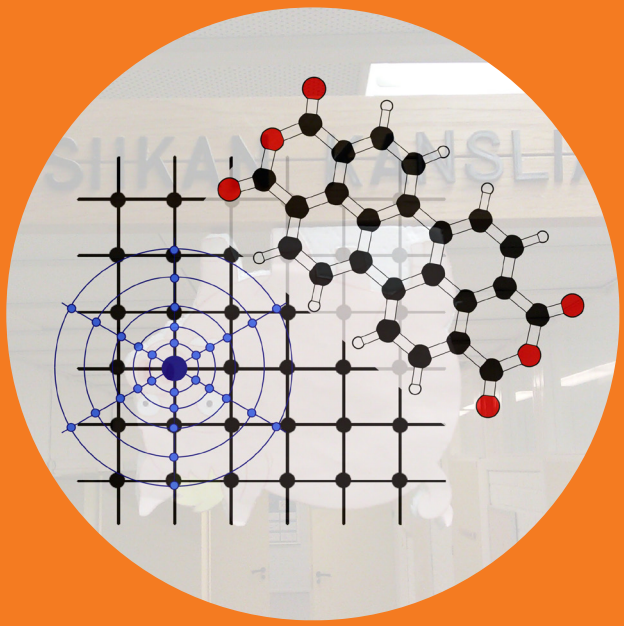

Aalto University

DOCTORAL DISSERTATIONS

Aalto University publication series
DOCTORAL DISSERTATIONS 6/2012

Van der Waals interactions in density-functional theory: implementation and applications

Andris Guļāns

Doctoral dissertation for the degree of Doctor of Science in Technology to be presented with due permission of the School of Science for public examination and debate in Auditorium K at the Aalto University School of Science (Espoo, Finland) on the 20th of January 2011 at 13 o'clock.

Aalto University
School of Science
Applied Physics
COMP

Supervisor
Prof. Martti J. Puska

Instructor
Prof. Martti J. Puska

Preliminary examiners
Prof. Juha Vaara, University of Oulu, Finland
Dr. Alexandre Tkatchenko, Fritz Haber Institute of the Max Planck Society, Germany

Opponent
Prof. Talat S. Rahman, University of Central Florida, United States of America

Aalto University publication series
DOCTORAL DISSERTATIONS 6/2012

ISBN 978-952-60-4471-2 (printed)
ISBN 978-952-60-4472-9 (pdf)
ISSN-L 1799-4934
ISSN 1799-4934 (printed)
ISSN 1799-4942 (pdf)

Unigrafia Oy
Helsinki 2012

Finland

The dissertation can be read at http://lib.tkk.fi/Diss/

441 697
Printed matter

Aalto University

Abstract

Aalto University, P.O. Box 11000, FI-00076 Aalto www.aalto.fi

Author
Andris Guļāns

Name of the doctoral dissertation
Van der Waals interactions in density-functional theory: implementation and applications

Publisher School of Science

Unit Applied Physics

Series Aalto University publication series DOCTORAL DISSERTATIONS 6/2012

Field of research Electronic structure theory

Manuscript submitted 3 October 2011 **Manuscript revised** 14 November 2011

Date of the defence 20 January 2012 **Language** English

☐ **Monograph** ☒ **Article dissertation (summary + original articles)**

Abstract

The density functional theory is, in principle, an exact ground-state method for interacting electrons. However, commonly applied local approximations make it severely unsuccessful for modelling materials where van der Waals interactions play a central role. The problem can be overcome by the van der Waals density-functional approach, which relies on a density functional with a built-in non-locality.

This Thesis reflects on efforts towards efficient numerical implementation of the approach and its application to a variety of problems such as molecule adsorption, self-assembly and defects in graphite. Surprisingly for the condensed-matter community, in cases where a molecule is attached to a surface by the "weak" van der Waals forces - they tend to be not so weak after all. These forces can seriously influence kinetics of various physical and chemical processes on surfaces or in layered solids. Hence, ignoring or mishandling the van der Waals interaction potentially leads to quantitatively and sometimes even qualitatively wrong results.

Keywords Density-functional theory, van der Waals interactions, physisorption, graphite.

ISBN (printed) 978-952-60-4471-2 **ISBN (pdf)** 978-952-60-4472-9

ISSN-L 1799-4934 **ISSN (printed)** 1799-4934 **ISSN (pdf)** 1799-4942

Location of publisher Espoo **Location of printing** Helsinki **Year** 2012

Pages 115 **The dissertation can be read at** http://lib.tkk.fi/Diss/

Preface

This Thesis has been prepared in the COMP Center of Excellence in Computational Nanoscience in Aalto University School of Science (formerly in Helsinki University of Technology) during the years 2006-2011.

I am grateful to my supervisors Professors Martti Puska and Risto Nieminen for patiently supporting me all these years and always providing a piece of advice whenever necessary. I thank all my other collaborators, especially, Professor Lev Kantorovitch, Professor Adam Foster and Dr. Arkady Krasheninnikov who were always interested in my work and presented opportunities to join their projects. Adam and Arkady are credited also for organising the inspirational workshops "Towards Reality in Nanoscale Materials" held every winter in Levi. I also appreciate the help from Simiam Ghan who assisted in polishing the Thesis. Special thanks go to the IT crew of our department and to CSC - IT Center for Science for maintaining computational resources, which were essential for this Thesis.

Espoo, January 2, 2012,

Andris Gulāns

Contents

List of Publications

This thesis consists of an overview and of the following publications which are referred to in the text by their Roman numerals.

I Andris Gulans, Martti J. Puska and Risto M. Nieminen. Linear-scaling self-consistent implementation of the van der Waals density functional. *Physical Review B*, 79, 201105, July 2009.

II O. H. Pakarinen, J. M. Mativetsky, A. Gulans, M. J. Puska, A. S. Foster and P. Grutter. Role of van der Waals forces in the adsorption and diffusion of organic molecules on an insulating surface. *Physical Review B*, 80, 085401, August 2009.

III M. Mura, A. Gulans, T. Thonhauser and L. Kantorovich. Role of van der Waals interaction in forming molecule-metal junctions: flat organic molecules on the Au(111) surface. *Physical Chemistry Chemical Physics*, 12, 4759, February 2010.

IV Karen Johnston, Andris Gulans, Tuukka Verho and Martti J. Puska. Adsorption structures of phenol on the Si(001)-(2×1) surface calculated using density functional theory. *Physical Review B*, 81, 235428, June 2010.

V Andris Gulans, Arkady V. Krasheninnikov, Martti J. Puska and Risto M. Nieminen. Bound and free self-interstitial defects in graphite and bilayer graphene: A computational study. *Physical Review B*, 81, 235428, July 2011.

Author's Contribution

Publication I: "Linear-scaling self-consistent implementation of the van der Waals density functional"

The author has designed and programmed the algorithm described in the article, performed all calculations and has written the first draft of the article.

Publication II: "Role of van der Waals forces in the adsorption and diffusion of organic molecules on an insulating surface"

The author has performed all vdW-DF calculations using his program developed for Publication I. He has also participated in discussions and editing of the paper.

Publication III: "Role of van der Waals interaction in forming molecule-metal junctions: flat organic molecules on the Au(111) surface"

The author has provided his program to other authors and performed a part of vdW-DF calculations. The author has also performed all MP2 calculations and participated in discussions and editing of the paper.

Publication IV: "Adsorption structures of phenol on the Si(001)-(2×1) surface calculated using density functional theory"

The author has performed the majority of calculations of adsorption energies and all transition state calculations. The author also has written roughly a half of the publication text.

Publication V: "Bound and free self-interstitial defects in graphite and bilayer graphene: A computational study"

The author has performed all calculations and has written the first draft of the paper.

The American Physical Society and The Royal Society of Chemistry (RSC) are acknowledged for allowing me to include published articles in this Thesis. Particularly, Publication III is reproduced by permission of the PCCP Owner Societies and is available on the RSC's website http://pubs.rsc.org/en/Content/ArticleLanding/2010/CP/b920121a.

1. Introduction

During past several decades the evolution of methods of computational materials science was guided towards accurate *ab initio* thermochemistry [1, 2]. The ultimate goal is to reach a precision matching the uncertainty of experiment. While objects of study as well as equipment for measurements may differ, the common convention is to declare the uncertainty equal to 1 kcal/mol (43 meV), which is known as "chemical accuracy" [1]. Among theoretical methods, only a few can guarantee such an accuracy, which, unfortunately, comes at an enormous expense and only the smallest systems can be studied in this manner. Anything larger than that has to be studied with cheaper and less accurate methods.

A popular compromise between the accuracy and the cost is the density functional theory (DFT), which is a feasible approach for a wide range of problems. Approximations, developed to make this method tractable, work well enough and DFT is extremely useful in various application, but some phenomena still remain especially difficult to describe. One of such problem cases is the van der Waals (vdW) interaction, which is recognised to be important not just for new industrial devices, but also for life itself. Approximations within DFT that have been successfully used during several decades turn out unreliable for the vdW interaction. In an attempt to resolve this issue, the Rutgers-Chalmers collaboration led by D. C. Langreth and B. I. Lundqvist has produced a new approach within DFT. Although it proved its usefulness almost immediately, there was a temporary obstacle that disallowed its application to a large number of problems. The most obvious implementation of the method is too expensive, while alternative algorithms did not exist in the beginning.

This Thesis is focused on a design of an efficient numerical implementation, which is applied to a range of problems where the vdW interactions are expected to be important. The applications in the Thesis include

physisorption of planar molecules on crystalline surfaces, dissociative adsorption of phenol on a silicon surface and defect phenomena in graphite.

2. Theoretical background

2.1 Electron correlation

The world of computational materials science is divided among a number of methods that allow for the explanation or even prediction of properties of various substances. The most sophisticated methods are derived from the Schrödinger equation and take into account electronic structure effects. These approaches, applied to a large number of problems, have two main streams: quantum chemistry (QC) and DFT [3]. The typical agenda in QC calculations is (i) solve the Hartree-Fock equations (one-electron problem), (ii) use the solution either to apply many-body perturbation theory or configuration interaction methods in order to approach the exact answer. Step (ii) introduces the picture in which electrons are not independent, but rather intimately correlated. Hence the energy improvement in step (ii) over step (i) is known as the correlation energy.

The practical approach to DFT, in turn, is based on solving the Kohn-Sham equations [4], which, in principle, allow us to obtain the electron density that minimises the total energy and corresponds to the ground state. This is achieved by replacing the real problem by a simplified one with non-interacting electrons moving in an external effective potential that guarantees the correct ground-state density and energy. The effective potential consists of an electrostatic term and whatever remains, which is known as the exchange-correlation potential. The latter part is normally approximated by local functions of density and/or its derivatives. Unfortunately, this scheme does not provide an opportunity of a systematic improvement of DFT energies, densities and other observables towards the exact ones.

The reason for the approximation in DFT is the high complexity of the exact exchange - correlation energy, which, at least at the moment, can-

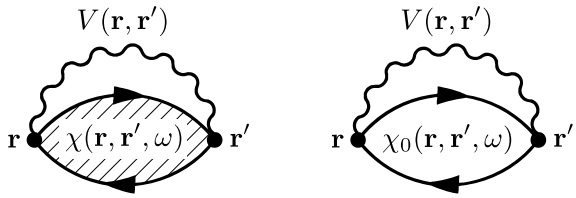

Figure 2.1. Diagrammatic representation of Eq. 2.2. The diagrams with shaded and empty bubbles correspond to fully interacting and non-interacting linear response functions, respectively.

not be directly expressed as a functional of density. Instead, using the adiabatic-connection fluctuation-dissipation theorem (ACFDT) [5, 6] it can be written as a functional of one-electron orbitals

$$E_{\rm xc} = -\int d^3r d^3r' \int_0^\infty \frac{du}{2\pi} \int_0^1 \frac{d\lambda}{\lambda} (\chi_\lambda(\mathbf{r},\mathbf{r}',iu)V_\lambda(\mathbf{r},\mathbf{r}') - n(\mathbf{r})\delta(\mathbf{r}-\mathbf{r}')), \quad (2.1)$$

where $n(\mathbf{r})$ is the electron density and $V_\lambda(\mathbf{r},\mathbf{r}') = \frac{\lambda}{|\mathbf{r}-\mathbf{r}'|}$ is the electron-electron repulsion potential scaled by the coupling strength λ. The orbital dependence enters Eq. 2.1 through $\chi_\lambda(\mathbf{r},\mathbf{r}',\omega)$, the non-local frequency-dependent full Kubo density-response function.

The correlation energy is singled out from Eq. 2.1 if χ_λ is replaced by the non-interacting response function $\chi_{\lambda=0}$. In that case, Eq. (2.1) becomes equal to the exchange energy $E_{\rm x}$. The correlation energy $E_{\rm c}$ is expressed through the difference $E_{\rm xc} - E_{\rm x}$ as

$$E_{\rm c} = -\int d^3r d^3r' \int_0^\infty \frac{du}{2\pi} \int_0^1 \frac{d\lambda}{\lambda} (\chi_\lambda V_\lambda - \chi_0 V_\lambda). \quad (2.2)$$

Eqs. (2.1) and (2.2) are derived in the framework of the many-body perturbation theory, where it is common to use diagrams in order to give intuitive flavour to the complicated integral expressions. Along these lines the two terms of Eq. 2.2 can be represented by the diagrams shown in Fig. 2.1.

2.2 van der Waals interaction

2.2.1 Many-body picture

A typical model system to illustrate the van der Waals (vdW) interaction is a complex of two fragments of matter with non-overlapping electron densities with no permanent electrical multipoles. For instance, it can be a dimer of noble-gas atoms or jellium layers, however, in the majority of

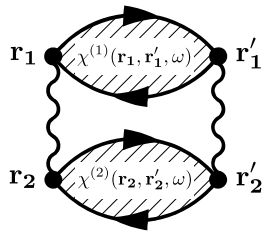

Figure 2.2. Diagrammatic representation of Eq. 2.3.

real materials one cannot guarantee the complete absence of the regular electrostatic interactions. Nevertheless, every quantum system with electrons has charge fluctuations that results in instantaneous polarisation and hence is responsible for the vdW attraction. The coupling of the fluctuations can be described by the means of the linear response using the many-body perturbation theory [7, 8]. Then, the vdW energy to the second order in electron-electron interaction is

$$E^{(2)} = -\int d^3r_1 d^3r'_1 d^3r_2 d^3r'_2 \int_0^\infty \frac{du}{2\pi} \frac{\chi^{(1)}(\mathbf{r_1}, \mathbf{r'_1}, iu)\chi^{(2)}(\mathbf{r_2}, \mathbf{r'_2}, iu)}{|\mathbf{r_1} - \mathbf{r_2}||\mathbf{r'_1} - \mathbf{r'_2}|}, \quad (2.3)$$

where $\chi^{(1)}$ and $\chi^{(2)}$ are the full interacting linear-response functions of the two fragments considered separately. The interaction energy can be expressed in terms of Goldstone-Feynman diagrams [9] as shown in Fig. 2.2.

Eq. 2.3 can be derived also using the ACFDT (Eq. 2.2) as the starting point. The comparison of Eqs. 2.2 and 2.3 reveals that they have a set common terms, which are sometimes called spectator diagrams. This concept means that the energy diagrams can be split into parts attributed to the non-overlapping regions by cutting interaction lines. This observation underlines the genuine non-locality and the many-body nature of the van der Waals interaction. Since the exchange interaction in the ACFDT is represented by the $\chi_0 V$-term, i. e.., the single bare bubble closed by the interaction line, and Eq. 2.3 does not contain it, it is apparent that the exchange does not contribute to the vdW attraction. In other words, the Hartree-Fock approximation completely misses the vdW interaction.

To recover the vdW interaction the correlation energy has to be calculated. One of the simplest and most common methods to do it is the Møller-Plesset perturbation theory to the second order, known simply as MP2. In this approximation, the correlation energy is calculated as

$$E^{\mathrm{MP2}} = \sum_{i<j} \sum_{a<b} \frac{[(ij|ab) - (ij|ba)]^2}{\varepsilon_i + \varepsilon_j - \varepsilon_a - \varepsilon_b}, \quad (2.4)$$

where the summation is carried over occupied (vacant) one-electron states

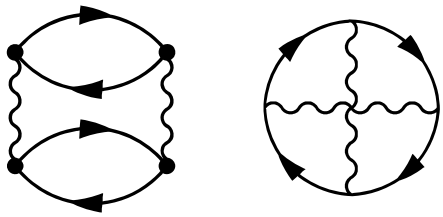

Figure 2.3. Diagrams included in the MP2 correlation energy. The direct (on the left) and the second-order exchange (on the right) terms do not contain any type of screening.

for the dummy variables i and j (a and b), the symbol $(ij|ab)$ denotes electron repulsion integrals. It is defined as $(ij|ab) = \int\int \varphi_i(\mathbf{r})\varphi_j(\mathbf{r}')\varphi_a(\mathbf{r})\varphi_b(\mathbf{r}')/|\mathbf{r}-\mathbf{r}'|d^3r d^3r'$. $\varphi_i(\mathbf{r})$ and ε_i are one-electron Hartree-Fock orbitals and corresponding eigenenergies, respectively.

The MP2 correlation energy can be represented diagrammatically as shown in Fig. 2.3. While the second-order exchange diagram (see Fig. 2.3) is not a spectator diagram, the bubble-bubble diagram has a very similar look to Fig. 2.2. The only difference is that the linear response functions ("the bubbles") in Fig. 2.3 are bare and not fully interacting. MP2 contains just the simplest diagrams among those responsible for the vdW attraction and misses such important aspects of many-body phenomena such as screening three-body interactions. Nevertheless, the results obtained with MP2 in practice are not necessarily bad. On the contrary, benchmark calculations of Jurečka *et al.* [10] have shown that for noncovalently bound molecular complexes where the bonding is dominated or matched by electrostatic interactions, MP2 produces reasonable binding energies.

To achieve better accuracy and to avoid the deficiencies of MP2, more elaborate *ab initio* methods are available. For instance, MP3 and MP4 (the third and fourth order many-body perturbation theories) and the coupled-cluster methods [11, 9] (which can be considered as the perturbation theory to the infinite order with only certain types of diagrams included) contain more components relevant for the vdW interaction. Unfortunately, these approaches are computationally very demanding and are prohibitively expensive in too many cases. In fact, even MP2 is currently too costly for a wide range of applications that includes adsorption of molecules on crystalline surfaces. Moreover, MP2 is applicable only to insulators, as Eq. 2.4 diverges for metallic systems.

2.2.2 Local and semilocal DFT methods

DFT as an alternative to the *ab initio* quantum chemistry methods has become the most used method in the electronic structure theory. Such an appreciation of DFT stems from its low computational complexity and the very resonable accuracy, which is determined by the approximation to the exchange-correlation energy functional $E_{\mathrm{xc}}[n]$. The simplest of them is the local density approximation (LDA), where

$$E_{\mathrm{xc}}^{\mathrm{LDA}}[n] = \int \epsilon_{\mathrm{xc}}(n(\mathbf{r}))n(\mathbf{r})d^3r. \tag{2.5}$$

The energy density ϵ_{xc} is a function of the electron density n. The function is chosen to reproduce the exactly known energy of the uniform electron gas. This energy contains contributions from all Goldstone-Feynman diagrams, but LDA describes them in an average way that allows to discard the overwhelming complexity of the many-body theory. The price for the simplification is the limited accuracy of LDA, one aspect of which is reflected in thermochemistry benchmark studies [12]. On the other hand, LDA applied for vdW-bound systems often has led to reasonable results. However, such a success has wrong reasons – the binding arises from the exchange [13], while, as shown in Sec. 2.2.1, the vdW attraction stems from the correlation.

The efforts to improve LDA have lead to the generalised-gradient approximation (GGA) – another widely used approach to DFT. The GGA exchange-correlation energy reads as

$$E_{\mathrm{xc}}^{\mathrm{GGA}}[n] = \int \epsilon_{\mathrm{xc}}(n(\mathbf{r}), |\nabla n(\mathbf{r})|)n(\mathbf{r})d^3r, \tag{2.6}$$

where the energy density ϵ_{xc} is a semi-local function of electron density. "Semi-local" means that the locality of ϵ_{xc} in LDA is complemented by the information on the behaviour of the electron density in the vicinity of point $\mathbf{r}$, since the electron density is smooth almost everywhere and the density gradient allows to predict variations of the density near $\mathbf{r}$.

GGA leads to a number of improvements over LDA in a description of chemical bonds with a hardly noticeable additional computational effort compared to LDA. According to benchmarks, covalent bonds are described reasonably with LDA and even better with GGA. However, intermolecular interactions present difficulties to both approaches. The LDA and GGA formulations in Eqs. 2.5 and 2.6 imply that electrons at point $\mathbf{r_1}$ “know nothing" about electrons at point $\mathbf{r_2}$. Such a picture is the opposite of the

ideas presented by Eq. 2.3 and Fig. 2.2, which illustrate that the vdW interaction is essentially non-local.

2.2.3 Extensions of (semi)local DFT methods

LDA and GGA completely lack a mechanism for a description of the vdW interaction, but there are possibilities to add it in a pragmatic manner. The non-relativistic vdW interaction between two small molecules (closed-shell atoms) is predictable and has the asymptotic form

$$E \sim -C_6/r^6, \tag{2.7}$$

where r is the inter-molecular (inter-atomic) separation and C_6 is a material-dependent coefficient. This relation can be proved using Eq. 2.3 [14] and it holds universally for finite systems. Then the vdW interaction energy can be estimated as a sum of interatomic pairwise potentials in the form of Eq. 2.7. However, such a potential is divergent at $r = 0$ and, thus, is not generally applicable. It is possible to resolve the issue by multiplying Eq. 2.7 by a damping function so that the asymptotic form at $r \to \infty$ remains and the new potential is well-behaved at small r. The approach of adding an inter-atomic potential to the total DFT energy has been proposed in various forms, but the most prominent ones have been introduced by Grimme [15, 16, 17], Tkatchenko and Scheffler (TS) [18] as well as Becke and Johnson (BJ) [19, 20].

In the method by Grimme, known as DFT-D2 [16], the potential is written as

$$E_{\mathrm{vdW}} = -s_6 \sum_{i<j} \frac{C_6^{ij}}{\mathbf{r_{ij}}^6} \frac{1}{1 + e^{-d(r_{ij}/s_R R_{ij} - 1)}}, \tag{2.8}$$

where r_{ij} is the distance between the i-th and the j-th atoms. The prefactor s_6 is a fitted scaling parameter, which is material independent, but it is different for each version of GGA complemented by Eq. 2.8. The coefficients $C_6^{ij} = \sqrt{C_6^i C_6^j}$ introduce another degree of empirism through the constants C_6^i, which are tabulated for each element in the periodic table. Finally, the parameters $R_{ij} = R_i + R_j$ combine the tabulated emprical van der Waals radii R_i, which are used with the constants d and s_R to determine the behaviour of the damping function.

The DFT-D2 method is numerically extremely efficient and, in test calculations, produces accurate binding energies, especially if combined with some of the double hybrid functionals instead of GGA [17]. Unfortunately, this approach has a number of drawbacks. First, it lacks flexibility and

dependence on the electron distribution. Polarisabilities of molecules depends on electronic states, but the C_6 coefficients assigned for each atom are rigid. For instance, the method does not distinguish between di- and trivalent carbon atoms. This issue is addressed in the DFT-D3 [17], TS and BJ methods. The DFT-D3 method takes into account the chemical environment of each atom by assigning a coordination number. In TS, the C_6 coefficients are rescaled based on the charge distribution, while, in BJ, they are calculated on the basis of the exchange-hole model. Hence, in this family, BJ is the only method that uses completely non-empirical C_6 coefficients. Although these adjustments improve qualities of these methods, but it has never been shown convincingly that any of these approaches work accurately for solids. Second, the asymptotic rule of Eq. 2.7 does not always work for extended systems [21]. In principle, this limits the applicability of the method, but, in practice, the unusual asymptotics reveals itself only at large distances far beyond the typical vdW bonding distance [22]. Third, the performance of DFT-D2, DFT-D3, TS and BJ methods depends strongly on a choice of empirical parameters. A recent sensitivity analysis has shown that the main source of uncertainty in these calculations is sealed in the damping function [23]. This result implies that the adjustment of C_6 coefficients performed on-fly in the TS and BJ method is relatively unimportant, and one should concentrate on adjusting the van der Waals radii instead, as is it is done in DFT-D3. In any case, the faith in these methods reduces to the faith in the parameters used for the calculations.

2.2.4 The van der Waals density functional (vdW-DF)

Despite the deficiencies of LDA and GGA, the formulation by Hohenberg and Kohn does not have any restrictions on what type or range of interactions are included in the exact DFT. If non-locality were somehow built in the correlation functional, the dispersion interaction could be naturally described within such an approximation to DFT.

Langreth, Lundqvist and their collaborators have derived such a non-local correlation functional [24] known as the van der Waals density functional (vdW-DF). They used ACFDT as the starting point and splitted the correlation energy into two parts: the short- and long-range ones. The short-range part can be adequately described by a local or semi-local functional and typically LDA is used for this purpose. The long-range part,

however, is derived using a number of approximations, namely, (i) the so-called full potential approximation $\chi_\lambda \approx \chi_{\lambda=1}$, which is well-justified for the long-range interactions if they are dominated by terms included in the random-phase approximation, (ii) the plasmon-pole approximation that allows to relate the linear response functions to the electron density and (iii) the expansion of the correlation energy expression in powers of the dynamic structure factor. These simplifications are essential for removing the hidden orbital dependence in Eq. 2.2 and hence reducing its complexity. As a result, the long-rang part of the correlation energy $E_{\rm c}^{\rm nl}$ is expressed finally in the form:

$$E_{\rm c}^{\rm nl}[n] = \frac{1}{2}\int\int n(\mathbf{r})\varphi(\mathbf{r},\mathbf{r}')n(\mathbf{r}')d^3r d^3r', \tag{2.9}$$

where $\varphi(\mathbf{r},\mathbf{r}')$ is a kernel function. Its mathematical definition is given in Appendix A, where the numerical evaluation of the kernel function is also discussed.

The kernel function has an important property – its spatial dependence satisfies the relation $\varphi(\mathbf{r},\mathbf{r}') = \varphi\left(q_0|\mathbf{r}-\mathbf{r}'|, q_0'|\mathbf{r}-\mathbf{r}'|\right)$ with local scaling parameters $q_0 = q_0(\mathbf{r})$ and $q_0' = q_0(\mathbf{r}')$. For practical calculations, it is convenient to express the kernel function in terms different variables, namely, as $\varphi = \varphi(D,\delta)$ with $D = \frac{q_0+q_0'}{2}|\mathbf{r}-\mathbf{r}'|$ and $\delta = \frac{q_0-q_0'}{q_0+q_0'}$. This rearrangement makes the storage and plotting of the function simpler. Its shape in the new coordinates is shown in Fig. 2.4. Interestingly, the kernel function always decays as $1/D^6$ at large D. This results in a failure to recover unusual asymptotic power laws that may occur for interacting extended systems [21]. As discussed above, this is a harmless drawback for a wide range of applications, although it is important to acknowledge.

The local scaling parameter is defined as an estimate of the short-range part of the exchange-correlation energy density $\varepsilon_{\rm xc}^0 = -\frac{3}{4\pi}q_0$, where $\varepsilon_{\rm xc}^0 = \varepsilon_{\rm xc} - \varepsilon_{\rm c}^{\rm nl}$. While, for total energy calculations, the short-range part is written as

$$\varepsilon_{\rm xc}^0 = \varepsilon_{\rm x}^{\rm GGA} + \varepsilon_{\rm c}^{\rm LDA}, \tag{2.10}$$

the evaluation of q_0 requires a different approach. The GGA form of $\varepsilon_{\rm xc}^0$ provides a relatively small correction to the LDA part in Eq. 2.10 and that eventually leads to infinite static polarisabilities of atoms and molecules $\alpha(0) \propto \int n(\mathbf{r})/(q_0(\mathbf{r}))^4 d^3r$ [25]. This is circumvented by using the gradient expansion approximation

$$q_0(\mathbf{r}) = -\frac{4\pi}{3}\left(\varepsilon_{\rm xc}^{\rm LDA}(\mathbf{r}) - \varepsilon_{\rm x}^{\rm LDA}(\mathbf{r})\left[\frac{Z_{\rm ab}}{9}\left(\frac{\nabla n}{2k_{\rm F}n}\right)^2\right]\right), \tag{2.11}$$

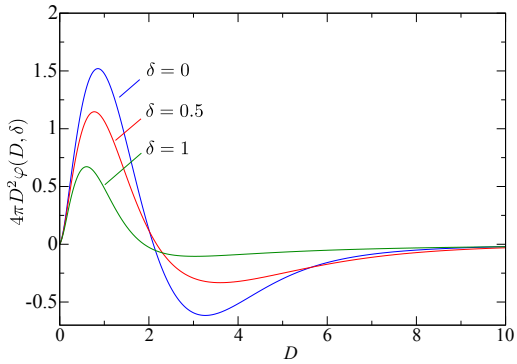

Figure 2.4. The kernel function of the vdW-DF.

where $k_{\mathrm{F}} = (3\pi^2 n)^{1/3}$ and $Z_{\mathrm{ab}} = -0.8491$. The term with the gradient correction grows unbounded at an exponential density decay and hence saturates the static polarisability integral. The prefactor Z_{ab} affects the polarisability and therefore also the accuracy of dispersion forces. The numerical value of the parameter is selected based on properties of the uniform electron gas. Z_{ab} corresponds to the gradient expansion coefficient that contains the contribution only from the "screened exchange" and does not contain anything from the "fluctuation" diagram that corresponds to essentially non-local interactions [26]. Such a choice proposed in Ref. [24] is debatable, since the derivation of the longe-range part of the correlation energy neglects the coupling-strength dependence in Eq. 2.2 and, thus, the "fluctuation" diagram cannot be accurately represented in the non-local correlation term of the vdW-DF. Moreover, it is not clear that the gradient expansion coefficients obtained for the uniform electron gas are useful in calculations of molecules.

A more recent analysis by Lee *et al.* suggests a different value for Z_{ab}, which is based on the large-N expansion and is not related to the uniform electron gas [27, 28]. This update of the parameter was one of the ingredients for revising the vdW-DF [28]. However, the link between the large-N expansion and Eq. 2.11 is obscure. It might have been expected that the reparametrisation should result in a non-local correlation functional, which is better suited for molecules than its predecessor. But recent calculations show that the update significantly worsens the accuracy of the vdW-DF for C_6 coefficents of close-shell atoms and small molecules [29]. This confirms that the new strategy of choosing Z_{ab} is also not so well justified.

The fact that the Z_{ab} can be chosen in two ways and non of them is rigor-

ously justified means that, strictly speaking, the vdW-DF method cannot be called *ab initio*, unlike its common acceptance in the DFT community. An alternative and more pragmatic approach is presented by Vydrov and van Voorhis in Ref. [25]. They also face the problem of choosing a numerical value of a polarisability-related parameter for their own non-local functional and solve it by fitting it in order to reproduce C_6 coefficients of individual atoms and small molecules.

Apart from the uncertainties of the non-local part of vdW-DF, there is no unique choice of $\varepsilon_{\mathrm{xc}}^{0}$ – the semi-local remainder of the exchange-correlation functional. The fundamental requirement for $\varepsilon_{\mathrm{xc}}^{0}$, especially for the exchange part, is a repulsive non-binding behaviour for complexes held together by the dispersion interaction. Although, in practice, GGA exchange functionals tend to provide binding, some of them are better behaved in this sense than the others. Since the revPBE exchange [30] showed very weak binding in test calculations, it was the recommended choice for the vdW-DF [24].

The sensitivity to the choice of the exchange functional and the lack of the consensus on the option add a certain degree of empirism to the method. However, in comparison to DFT-D2 and similar methods, the vdW-DF approach does not rely on material-dependent constants and automatically adjusts to variations in the electron density. In other words, the vdW-DF method inherits some of the flaws discussed in Sec. 2.2.3, but heals the others.

3. Numerical treatment of the vdW-DF

A typical DFT calculation involves several different steps and one of them is the evaluation of the exchange-correlation functional $E_{\mathrm{xc}}[n]$ and the related potential $v_{\mathrm{xc}}(\mathbf{r}) = \delta E_{\mathrm{xc}}/\delta n(\mathbf{r})$. Within the LDA and GGA approaches, this step is relatively inexpensive, especially for large problems, where efforts spent in linear algebra or other standard numerical routines are much more time consuming. Indeed, with the basis set size N, the form of Eqs. (2.5–2.6) implies the computational complexity $O(N)$, while typical routines, such as the full-diagonalisation and fast-Fourier transform require $O(N^3)$ and $O(N \log N)$ floating point operations, respectively. Some electronic structure codes, however, can benefit from a sparsity of matrices occuring in a course of a calculation or use other tricks to reduce their complexity and achieve the linear-scaling for the computational expense. Still, even then the evaluation of an exchange-correlation functional is not the major expense.

In the case of the vdW-DF, the three-dimensional integral of the semi-local part is complemented by a six-dimensional integral of the non-local part. Such an extension costs an additional effort, which can be overwhelming if the evaluation of the non-local correlation energy term is not implemented intelligently. The first algorithm described in literature and used in pioneering applications takes the most direct and straightforward route, which turned out to be costly and not very accurate. For obvious reasons, in this Thesis, it is referred to as the brute-force approach.

In the course of time, more elaborate methods have emerged including the adaptive real-space approach [31], which is described in this Thesis in detail. The convolution approach [32] and the Monte-Carlo algorithm [33] are among the other efficient alternatives, but they are not discussed here.

3.1 Brute-force approach

Suppose the electron density $n(\mathbf{r})$ is defined in a finite box and supplied on an evenly-spaced three-dimensional grid $\{\mathbf{r}_i\}$ with i ranging from 1 to the grid size N. Then the integral of Eq. 2.9 can be approximated using the definition of the Riemann integral

$$E_{\mathrm{c}}^{\mathrm{nl}}[n] \approx V_0^2 \sum_{i,j=1}^{N} n(\mathbf{r}_i)\varphi(\mathbf{r}_i, \mathbf{r}_j)n(\mathbf{r}_j), \tag{3.1}$$

where V_0 is the volume of the primitive element of the grid. This expression is equivalent to the trapezoid rule if the density vanishes at the boundaries of the box. The direct application of Eq. 3.1 leads to a computational effort that scales as $O(N^2)$. It means that a twofold increase in the resolution of the grid with a constant box size leads to a four times heavier calculation.

If the electron density $n(\mathbf{r})$ is a periodic function and it is supplied on a grid within a primitive unit cell, Eq. 3.1 is still applicable. Now, $E_{\mathrm{c}}^{\mathrm{nl}}$ has to be evaluated as the energy per unit cell and the index i still runs over N points of the cell. The other summation, however, is carried out over all space and j ranges over an infinite number of points. In practice, it is sufficient to consider a finite number of points M that is large enough to converge the sum. Typically $M > N$, which maintains the $O(N^2)$ scaling.

The algorithm can be slightly refined using the fact that $\varphi(D, \delta)$ decays rapidly at large D (or equivalently at large $|\mathbf{r}-\mathbf{r}'|$). Then it makes sense to define a cutoff length R_{c} such that if $|\mathbf{r}_i - \mathbf{r}'_j| > R_{\mathrm{c}}$ the corresponding term in the sum is disregarded. This simple trick introduces a linear scaling to the algorithm, since for each $\mathbf{r}_i$ only a fixed number of $\mathbf{r}_j$ have to be considered. For instance, if the grid spacing in a typical pseudopotential calculation is $d = 0.1$ Å and, without aiming at a high accuracy, $R_{\mathrm{c}} = 10$ Å is chosen, the introduced cutoff length leads to $M = 4\pi/3(R/d)^3 = 4.2 \cdot 10^6$. Since M is so large, such an evaluation of $E_{\mathrm{c}}^{\mathrm{nl}}$ brings an enormous overhead compared to a calculation of a GGA exchange correlation energy.

Unfortunately, the efficiency considerations are not the only concern. As discussed in Appendix A, $\varphi(\mathbf{r}, \mathbf{r}')$ is singular at $\mathbf{r} = \mathbf{r}'$ and hence it is not straightforward to decide what to do if $i = j$. Moreover, the trapeziodal rule is accurate only for smooth integrands, but $\varphi(\mathbf{r}, \mathbf{r}')$ varies rapidly at small $|\mathbf{r}-\mathbf{r}'|$ and has a region of interest determined by the local parameter $q_0(\mathbf{r})$ (see Fig. 2.4). In other words, the evenly-spaced grid is suitable to resolve all the features of the density, but it ignores the scales relevant for

the kernel function and hence is inappropriate for calculating the whole six-dimensional integral of Eq. 2.9.

3.2 Adaptive real-space approach

In Publication I, it is shown that the problems of the brute-force approach can be overcome simply by evaluating integral

$$\epsilon_{\mathrm{c}}^{\mathrm{nl}}(\mathbf{r}) = \frac{1}{2}\int \varphi(\mathbf{r},\mathbf{r}')n(\mathbf{r}')d^3\mathbf{r}' \tag{3.2}$$

in spherical coordinates with the origin at $\mathbf{r}$. Defining $\tilde{\mathbf{r}} = \mathbf{r}' - \mathbf{r}$ and $F(\tilde{\mathbf{r}}) = \varphi(\mathbf{r}',\mathbf{r})n(\mathbf{r}')$, Eq. 3.2 can be rewritten as

$$\epsilon_{\mathrm{c}}^{\mathrm{nl}}(\mathbf{r}) = \frac{1}{2}\int_0^\infty d\tilde{r}\int_0^\pi d\vartheta\int_0^{2\pi} d\phi\ \tilde{r}^2\sin\vartheta F(\tilde{r},\vartheta,\phi), \tag{3.3}$$

where the Jacobian $\tilde{r}^2\sin\vartheta$ immediately resolves the singularity issue.

Inspired by the procedure descibed in Ref. [34], the practical approach to evaluation of Eq. 3.3 is based on the Gauss-Chebyshev quadrature of the second kind for the radial part and the Lebedev quadrature for the angular part [35, 36]. However, to make the Gauss-Chebyshev quadrature applicable to Eq. 3.3 it is necessary to map the integration range $\tilde{r} \in [0;\infty)$ to $x \in [-1;1]$, where x is a new integration variable. The transformation

$$\tilde{r} = r_m\sqrt{\frac{1+x}{1-x}} \tag{3.4}$$

fulfills the requirement with r_m being an arbitrary positive constant. Eq. 3.3 is then approximated as

$$\epsilon_{\mathrm{c}}^{\mathrm{nl}}(\mathbf{r}) \approx 2\pi\sum_{i=0}^{N^{(r)}} w_i^{(r)}\frac{r_m^3}{(1-x_i)^3}\sum_{j=1}^{N^{(\Omega)}} w_j^{(\Omega)}F(\tilde{r}(x_i),\Omega_j). \tag{3.5}$$

The angular points Ω_j and their weights $w_j^{(\Omega)}$ are pretabulated. For the Gauss-Chebyshev grid points and corresponding weights, simple expressions exist

$$x_i = \cos\frac{\pi i}{N^{(r)}} \tag{3.6}$$

and

$$w_i^{(r)} = \frac{\pi}{N^{(r)}}\sin^2\frac{\pi i}{N^{(r)}}, \tag{3.7}$$

where $N^{(r)}$ is the size of the quadrature grid and $0 \le i \le N^{(r)}$.

Inserting all values of i where $0 \le i < N^{(r)}/2$ and $N^{(r)}/2 < i \le N^{(r)}$ into Eqs. 3.4 and 3.6 produces radial shells with $0 \le r_i < r_m$ and $r_m <$

$r_i < \infty$ in equal amounts. Thus, the transformation in Eq. 3.4 contains a mechanism to adjust the quadrature grid according to the scale of the kernel function, and setting $r_m = 1/q_0$ allows Eq. 3.5 to be equally useful low- and high-q_0 regions.

The effort required to calculate ϵ_c^{nl} with this method requires a number of floating point operations proportional to $N^{(r)}N^{(\Omega)}$, which is a number limited by convergence considerations and does not depend on N. For most of practical applications, especially when pseudo-densities are handled, the values $N^{(r)} = 50$ and $N^{(\Omega)} = 86$ guarantee a very high accuracy. A calculation of E_c^{nl} requires one evaluation of ϵ_c^{nl} in each of N grid points that settles the overall computational complexity to $O(N)$. This is the same scaling of the computational complexity as in the refined brute-force approach, but with a much smaller prefactor, since $N^{(r)}N^{(\Omega)} \ll M$.

The comparison of the two methods, however, is not that straightforward, because the brute-force approach uses the electron density only in predefined grid points, while the adaptive method requires an ability to evaluate the density at any point between the grid nodes. A convenient and efficient solution is interpolation, which is described in detail in Appendix B. Clearly, an interpolation is a slower process than just retrieving a number from a table, but the adaptive approach is still considerably faster than the brute-force method.

In comparison to a plain GGA calculation, the adaptive algorithm is still fairly expensive, but it is possible to make it cheaper by allowing $\epsilon_c^{nl}(\mathbf{r})$ to be evaluated with smaller quadrature grids at points where high enough accuracy can be achieved with smaller grids. For instance, the number of angular grid points $N^{(\Omega)}$ does not have to be the same for each radial shell and a predefined accuracy can be reached by adjusting (or adapting) $N^{(\Omega)}$ in each particular case. In computational chemistry, such an approach is known as grid pruning and is commonly used for multi-centre integration of the energy density in DFT calculations [37, 38]. Unfortunately, the experience accumulated in this field during two decades is not directly transferable for Eq. 3.5, since the spatial size of quadrature grids in computational chemistry packages is constant and the grid pruning is always the same. Here, on the other hand, the size of the quadrature grid needs to be constantly adjusted and the variation of the number of angular grid points is done on the fly. The detailed description how is it implemented in practice is presented in Appendix C.

To summarize, the adaptive real-space approach combines automatic

adjustment of quadrature grids on two different levels: i) the grids are stretched or compressed in the radial direction in order to follow the characteristic local length scale of the kernel function and ii) the numbers of radial shells and angular points are varied in order to avoid redundancy in calculations when smaller grids are good enough to achieve sufficient accuracy. In other words, the essence of this integration approach is to focus on evaluating the integrand of Eq. 3.2 at points that matter the most.

The adaptive real-space algorithm has been initially implemented as a stand-alone program for post-processing calculations. This program has been successfully applied for a number of applications [39, 40, 41, 42] that include also Publication IV. Unfortunately, an *a posteriori* calculation provides only the total energy, but not the Hellmann-Feynman forces. An implementation of forces requires a self-consistent treatment of vdW-DF. How to apply this algorithm for self-consistent calculations is explained in Appendix E. The method has been implemented in electronic structure codes SIESTA [43] and VASP [44]. The vdW-DF module within SIESTA has been applied in Refs. [31, 45, 46, 47](including Publications I, II and III) and a similar module within VASP has been used in Refs. [48, 49, 50, 51](including Publication V).

4. Applications

4.1 Non-covalent interactions of molecules

Non-covalent interactions are essential to explain various phenomena especially in organic and biochemistry. For instance, processes such as protein folding and replication of DNA are controlled by both intermolecular interactions with water and intramolecular interactions between parts of a protein or a DNA macromolecule. Interactions with or within macromolecules are difficult to study. Thus, the applicability of a certain DFT method can be assessed by considering smaller molecular units that contain the same or similar functional groups. For this purpose, several benchmark sets have been developed [10].

Qualities of the vdW-DF are studied in Publication I, where the method is applied for the S22 set [10], which consists of complexes of small molecules. This set contains cases where the binding energy is dominated by electrostatic forces, dispersion or a combination of the two. Such a mixture allows us to perform a quick test of a method for the main types of intermolecular interactions.

A particularly important question to ask in conjunction with the test calculations is whether the original recipe for the vdW-DF presents a well-rounded combination of approximations for the exchange and the correlation. For a comparison, the revPBE (the original choice in Ref. [24]) and PBE [52] exchange functionals are both applied in the study. The tests reveal that both selections follow the trends observed in the accurate CCSD(T) calculations by Jurečka *et al.* However, it turned out as well that the two variations of vdW-DF do not perform equally well for the three different classes of complexes. The PBE exchange yields accurate binding energies for the hydrogen-bonded dimers, while it significantly overbinds the other complexes. The same time, the revPBE is fairly ac-

curate for dispersion-bonded complexes, but significantly underestimates the strength of the hydrogen-bond.

The important conclusion from Publication I is that a large portion of the uncertainty in vdW-DF calculations comes specifically from the exchange. Dion *et al.* [24], as they introduced the vdW-DF method, emphasized that the most important requirement in this type of calculations is the absence of binding due to the semi-local exchange. Publication I stimulated a discussion that allowed the departure from this point of view and arrived at the conclusion that it is necessary to find a GGA exchange functional that contributes to the interaction energy in a similar manner as the exact exchange. Later on, vdW-DF has been revised and the adjustment of the exchange has been one of the key features in the recent improvements [28].

4.2 Physisorption of flat organic molecules

As nanotechnologies advance, organic molecules become increasingly important in the engineering of electronic devices. In attempts to decrease the size of circuit elements and to make their manufacturing more cost-efficient, organic molecules are considered as an alternative to silicon and other inorganic materials. Although some applications, for instance, organic light-emitting diodes, have already reached the global market and casual consumer, this industry still faces a number of challenges. In particular, it is important to understand details behind constructing a circuit with organic elements in it. This typically involves self-assembly, which has to be somehow controlled. Controlling such a process requires a detailed (both qualitative and quantitative) understanding of phenomena behind it.

A typical self-assembly process on a crystalline surface can be described by the key features shown in Fig. 4.1. Molecules are deposited on a cleaned and possibly also otherwise prepared surface. For any kind of a self-organisation the deposited molecules are required to be mobile. For instance, the ”weak” vdW interaction can keep the molecules firmly attached to the surface, but it hardly resists lateral motion. The molecules move then in a quasi-two-dimensional space, where they can meet each other. An agglomeration starts if the interaction between the molecules is attractive and sufficiently strong, which can be arranged via hydrogen

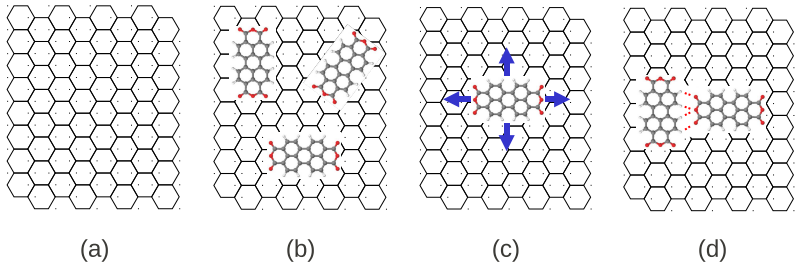

Figure 4.1. Four stages of forming a self-assembled structure on a crystalline surface: (a) a clean surface, (b) deposition of molecules on the surface, (c) diffusion of molecules, (d) agglomeration of molecules into islands (two-dimensional clusters).

bonding.

The described self-assembly process is determined by non-covalent interactions and therefore it is difficult to investigate by means of (semi-)local density functionals. In Publications II and III, it is shown that PBE severely underestimates the binding of planar organic molecules (melamine, NTCDA and PTCDA, shown in Fig. 4.2) to the KBr (001) and Au (111) surfaces. The adsorption energies are very low and range from -0.10 to -0.51 eV (Table 4.1). To appreciate it, these values can be inserted into the Arrhenius equation for the reaction rate k

$$k = A \exp(-\frac{E_a}{k_B T}), \tag{4.1}$$

where E_a, k_B, A and T are activation energy, Boltzmann constant, trial rate (also known as the pre-exponential factor) and temperature, respectively. Assuming $A = 10^{12}$–10^{13} s^{-1}, which is the typical magnitude of the trial rate, and setting E_a equal to any of the above adsorption energies, the typical desorption time at room temperature is $1/k \ll 1$ s. The same time it is known that these molecules are well-attached to the surfaces at these conditions [53, 45].

In an attempt to confirm that the disagreement between experiment and the DFT calculations can be explained by the neglect of the vdW interaction, the vdW-DF is applied to the adsorption problem in Publications II and III. The results summarised in Table 4.1 show that the vdW-DF recovers the missing part of the binding energy and predicts a three- to ten-fold increase in the adsorption energy as compared to PBE. Noteworthy, the strength of the interaction between a surface and a molecule depends on the size of the latter. The adsorption energies of melamine, NTCDA and PTCDA on Au(111) relate as 1.4:1.0:0.7, while the numbers of their atoms

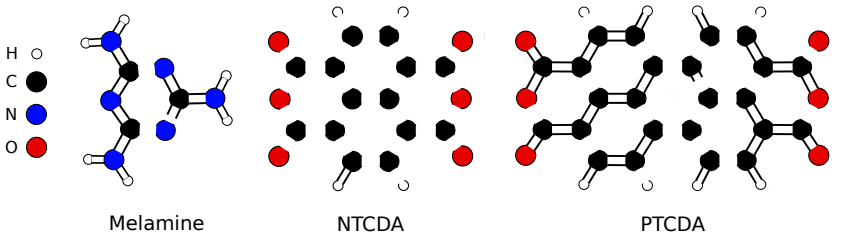

Figure 4.2. Structure of studied molecules: Melamine(1,3,5-triazine-2,4,6-triamine), NTCDA (naphthalene tetracarboxyldianhydride) and PTCDA (perylene-3,4,9,10-tetracarboxylic-3,4,9,10-dianhydride).

Table 4.1. Adsorption energies (eV) of flat organic molecules on the KBr (001) and Au (111) surfaces. The number in parentheses corresponds to a vdW-DF(PBE) calculation.

Molecule	Substrate	PBE	vdW-DF(revPBE)
Melamine	Au(111)	0.25	0.88
NTCDA	Au(111)	0.10	1.31
PTCDA	Au(111)	0.17	1.88
PTCDA	KBr (001)	0.51	1.80(2.36)[1]

relate as 1.6:1.0:0.7. This observation is roughly in agreement with the naïve picture that the vdW interaction can be described as a superposition of pair-wise atomic interactions. At the same time, the PBE adsorption energies do not show such a correlation.

In addition to the adsorption energy, the non-covalent forces can also affect the diffusion dynamics on a surface. Particularly, the migration energy for a PTCDA molecule on the KBr(001) surface is 0.4 or 0.3 eV depending whether or not the vdW interaction is neglected or included in the calculation. In both cases the height of the energy barrier is determined by a well-structured distribution of charge on the surface of the alkali halide. The opposite trend is observed on the Au (111) surface, where all atoms represent the same chemical species and valence electrons are distributed almost uniformly. The calculated migration energy for PTCDA is then only 0.05 eV regardless of the method used.

On both surfaces considered, PCTDA molecules are mobile at room temperature and can form self-assembled structures. The first step of this process is dimerisation, and it has been studied in Publication III. The structures of the considered molecule dimers are shown in Fig. 4.3. In all cases, the origin of binding is a hydrogen bond, but only the melamine

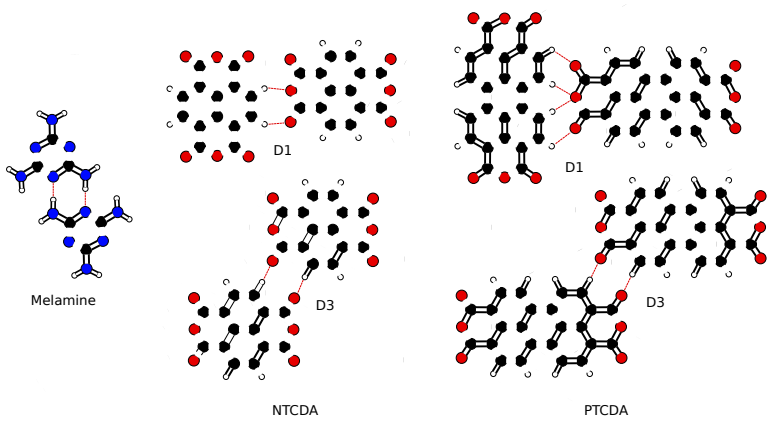

Figure 4.3. Studied dimer structures.

Table 4.2. Dimer binding energies (eV) of flat organic molecules in the gas phase. Dimers of NTCDA and PTCDA are labelled according to the nomenclature introduced in Fig. 4.3.

Dimers	PBE	vdW-DF(revPBE)	MP2
Melamine	0.48	0.42	0.49
NTCDA (D1)	0.06	0.18	0.19
NTCDA (D3)	0.16	0.28	0.28
PTCDA (D1)	0.23	0.38	0.45
PTCDA (D3)	0.25	0.38	0.35

dimer is held together by a strong hydrogen bond ($N-H\cdots N$), where electrostatic forces dominate. The attraction in the NTCDA and PTCDA dimers, in turn, is due to a weak hydrogen bond ($C-H\cdots O$), where according to Ref. [54] the roles of the electrostatic and vdW components is equally important. These considerations raise concerns that GGA functionals are not suitable for this type of systems. To test this, PBE as a representative of GGA has been applied for the structures along with vdW-DF and MP2, the methods that are expected to provide a reasonable benchmark.

The comparison of the dimer binding energies shown in Table 4.2 reveals that, indeed, the GGA method performs well for the intermolecular interactions only in the melamine dimer. For the other molecules, the strength of the binding is noticeably underestimated. Thus, the semi-local approach is not applicable even for the molecules gas-phase. The other two methods, the vdW-DF and MP2, yield similar, yet not identical

interaction energies. This is not a surprise knowing the mild disagreement between the two methods for the S22 benchmark set.

Finally, in self-assembly studies, it is important to know how the presence of a surface influences the interaction between molecules. This question is addressed in Publication III, where the melamine dimer on the Au(111) is considered. According to the vdW-DF calculation, the binding energy obtained with respect to the isolated surface and two individual melamine molecules is 2.08 eV. On the other hand, if the same quantity is calculated using the numbers obtained for pairwise interactions (melamine–melamine and melamine–Au(111)), nearly the same answer, i.e. 2.18 eV, is obtained. This hints that the dynamics of the self-assembly of melamine and the other two flat organic molecules on the Au(111) surface can be studied by considering exclusively a two-dimensional pool of molecules and neglecting the surface. On the other hand, the study of the diffusion of PTCDA molecules on KBr(001) revealed a quite "bumpy" potential energy surface with the migration energy of 0.4 eV, which is comparable to the interaction energy within a PTCDA dimer. In this case, the presense of the surface cannot be entirely neglected.

In conclusion, Publications II and III have shown the dominant role of the dispersion interaction in the adsorption of the planar organic molecules on the considered surfaces. Interactions between molecules are determined by hydrogen bonds, which are a complex combination of electrostatic, vdW and even covalent interactions. In structures with a weak hydrogen bond, the vdW component becomes increasingly important. This component missed in PBE is recovered with the vdW-DF, which shows similar trends in results as MP2.

4.3 Adsorption of phenol on silicon (001)

Attempts to improve electronic devices based on silicon are directed towards reducing the size of circuitry and thereby lowering the power consumption and making electronic devices faster and cheaper to manufacture. The minituarisation, in fact, came so far that the surface effects become increasingly important and the performance of the devices may depend on the ways how the surface is protected. This is achieved by producing semiconductor coatings and the prominent route is to functionalise the surface by organic molecules. Moreover, organic substances exhibit a

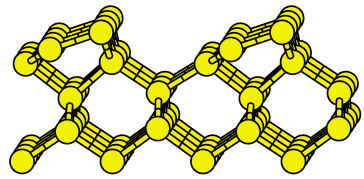

Figure 4.4. (2×1) reconstruction of the Si(001) surface.

vast variety of physical and chemical properties that can complement regular silicon-based electronics with new or simply improved properties.

Organic chemistry provides an enormous stock of diverse molecules, which are different in shape, size and chemical and physical properties. In Publication IV, we have studied a particular case – the adsorption of phenol on the Si(001)-(2×1) surface (see Fig. 4.4). However, the interaction of organic molecules with an inorganic semiconductor surface is mainly determined by their constituent functional groups and phenol can be considered also as a prototype for larger molecules with the phenoxy group at one of its ends.

The Si (001) surface reconstructs to minimise the number of dangling bonds, but even then it remains highly reactive. As a result, phenol chemisorbs to it and even dissociates. This is not a stereotypical "weakly" interacting vdW system, although, in principle, the long-range dispersion forces can influence even covalently bound systems. For instance, Johnston *et al.* have used this argument in Ref. [55] to explain why experiment and GGA calculations disagree on which is the energetically preferable chemisorption configuration of benzene on the Si(001)-(2×1) surface.

Keeping in mind that the accurate description of both covalent and non-covalent interactions is important, the adsorption of phenol is considered in Publication IV using a number of exchange-correlation functionals, including vdw-DF. The adsorption energies obtained for a variety of structures are shown in Fig. 4.5. Regardless of the method applied, dissociation is strongly favoured. Splitting off a proton (in structures labelled as D–F in Fig. 4.5) or a whole hydroxyl group (C in Fig. 4.5) lead to a gain in the energy of 1–3 eV. These results are consistent with the experimental findings of Ref. [56], where dissociation of phenol was observed.

The phenol molecule in the several states (A, B, E and F in Fig. 4.5) takes a lot of space on the surface, namely, it occupies two surface Si dimers. On the other hand, after dissociation, the molecules can populate the surface

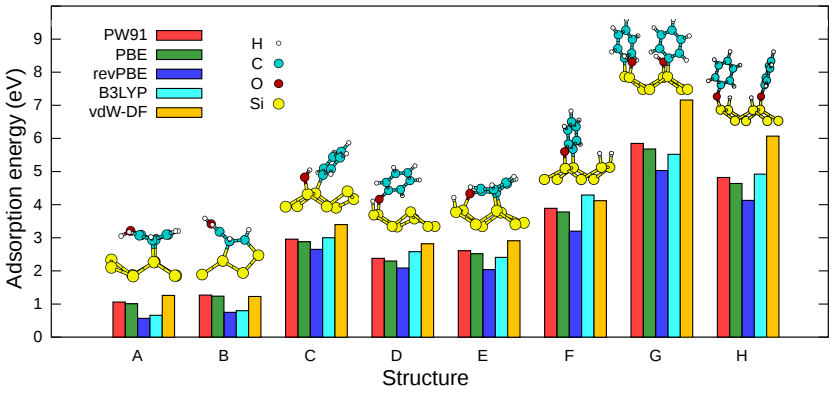

Figure 4.5. Structures of phenol adsorbed on the Si(001)-(2×1) surface and the corresponding adsorption energies per surface unit cell. Structures A–F correspond the coverage of 0.25 molecules per one surface Si atom, while for structures G and H it is 0.5 molecules per one surface Si atom.

twice as densely (G and H in Fig. 4.5). In this case, adsorbed molecules interact directly with each other and the type of the interaction depends on the exchange-correlation functional applied. PW91 [57], PBE, revPBE and B3LYP [58] predict a repulsion, while the vdW-DF – an attraction. The source of the discrepancy is the inability of the former four functionals to describe the vdW interaction. This deficiency does not affect the qualitative conclusion that, at high exposures to the phenol vapour, it is energetically favourable to saturate each Si dimer by its own phenol molecule. However, the highest surface coverage is unlike if the molecules interact repulsively. Then regardless of the phenol vapour density and exposure times, the outcome is a double dissociation of the molecules (F in Fig. 4.5) that is the energetically preferable scenario at low surface coverages. On the other hand, if the vdW interaction is included in the calculation the highest surface coverage is possible to achieve at certain conditions.

The results summarised in Fig. 4.5 show a clear disagreement among the DFT methods. The energies of each particular adsorption structure are dispersed within 0.5–2.1 eV, which shows that there is still a long way towards the quantitative computational surface chemistry. One of the reasons why we are not there yet is the difficulty to handle the long-range dispersion effects that reveal themselves even despite the strong covalent nature of bonding.

While desorption energies of phenol on the Si(001)-(2×1) surface have not been measured, an experimental study [56] has shown that at different exposures of phenol vapour the adsorbed molecules undergo dissocia-

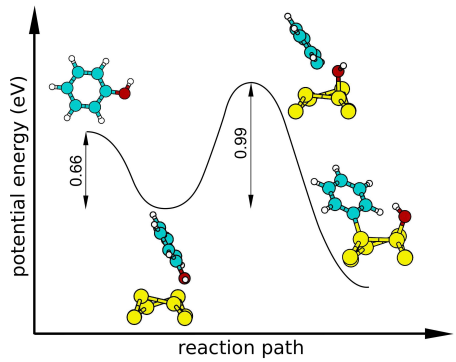

Figure 4.6. Schematic of structural transformations leading to a separation of the hydroxyl group from phenol on the Si (001)-(2×1) surface.

tion into hydrogen atoms and a phenoxy- groups(D and H in Fig. 4.5). This conclusion leans on an interpretation of the X-ray photoemission spectroscopy (XPS) giving knowledge about chemical environment of atoms.

At first sight, the experimental data contradict results reported in Fig. 4.5. However, the phenol chemistry on this surface is fairly rich, and there are chemically inequivalent adsorption structures with certain similarities among themselves. Thus, it is reasonable to question how well they can be resolved via XPS. To understand this, their spectra were simulated in Publication IV. It turned out that all structures with a hydrogen atom dissociated from the phenoxy group (D–F and H in Fig. 4.5) yield nearly indistinguishable spectra if the broadening of the lines is the same as in Ref. [56]. Moreover, it turned out that structures with the separated hydroxyl group (C and G in Fig. 4.5) can, in principle, be present as a satellite. Based on these computational results, the only firm conclusion that can be deduced from the XPS experiment is the dissociation of phenol.

For a better insight, structural transformations of phenol on the Si(001)-(2×1) surface are considered in Publication IV. Some of the considered adsorption structures can be separated from others by high energy barriers and hence would be unlikely to observe in a real-life experiment. The kinetics of the transformations is determined by the Arrhenius equation (see Eq. 4.1), where the key quantity is the activation energy. To determine it, a search for a transition state (TS) of corresponding reactions has been performed using the adaptive nudged elastic band method as described in Ref. [59].

As a phenol molecule approaches the surface, initially it becomes attached non-covalently (physisorbed) in what is known as a precursor state.

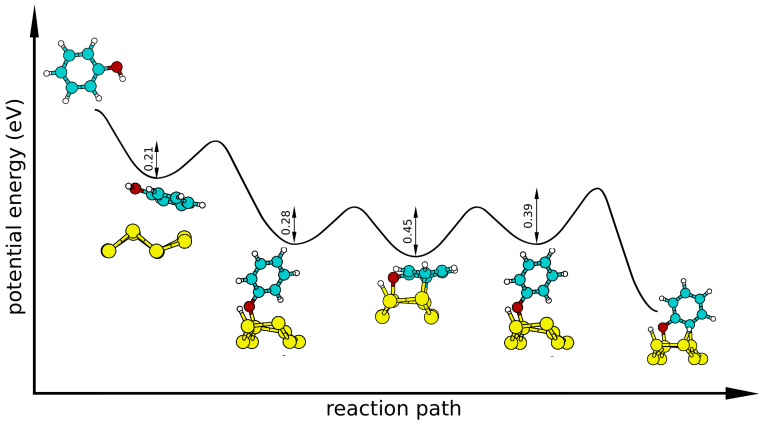

Figure 4.7. Schematic of structural transformations that lead to double dissociation of phenol on the Si (001)-(2×1) surface. The sequence of structures is a gas-phase phenol molecule $\rightarrow$ a precursor state $\rightarrow$ D $\rightarrow$ E $\rightarrow$ D $\rightarrow$ F (see also Fig. 4.5).

In this case, saturation of dangling bonds is not involved and the adsorption energy in the precursor states is 0.2–0.7 eV, which is lower than for any of the structures shown in Fig. 4.5. After the molecule is physisorbed, it can either return back to the gas phase or promote the strength of its bond with the surface from a weak vdW bond to the covalent one. Which of the two processes dominates depends entirely on the corresponding activation energies. In particular, a separation of a whole hydroxyl group turns out to be very unlikely, since the desorption from a precursor state requires 0.66 eV, whereas the dissociation energy is 0.99 eV, as illustrated in Fig. 4.6. To give an intuitive meaning to the difference in these energies, it is instructive to insert it into the Arrhenius equation that yields the ratio of reaction rates of 10^5 at room temperature. In other words, on average only one molecule out of 10^5 overcomes such a dissociation barrier.

In a different precursor state, the phenol molecule aligns itself in a way suitable for splitting the O–H bond. According to the TS calculations, this type of dissociation requires less energy than desorption. This qualitative difference in the energetics of the two different dissociation scenarios clearly explains the XPS data of Ref. [56] that contain hints of a split-off proton and does not prompt the presence a separated hydroxyl group.

The calculated potential energy surface landscape (shown in Fig. 4.7) favours also a secondary dissociation of phenol. The corresponding energy barrier is as low as 0.39 eV, which can be easily surpassed at room temperature. Consequently, double dissociation is expected to occur at

least in conditions of shortage of the phenol vapour. If the surface is exposed to a large dose of phenol, it is also possible that the time necessary for the second dissociation is too long and uncovered Si atoms on the surface rather bond with other molecules. As the vdW-DF calculations have shown, the resulting interaction between phenol molecules on the surface at high coverages is attractive and the formation of precursor states next to previously adsorbed molecules would be energetically favourable. If appropriate precursor states are occupied, the energetically inexpensive cleavage of the O–H bond is expected to occur.

In conclusion, the calculations in Publication IV reveal the complexity of the adsorption of phenol on the Si(001)-(2×1) surface. The previous interpretation of the XPS data has been proved to be poorly justified and determining the final adsorption state requires the analysis of kinetics. The transition state calculations have shown two possible scenarios: a double dissociation of phenol molecules and a single dissociation of the hydroxyl group at the conditions of excess phenol. In the latter case, dissociated phenol molecules populate densely the surface. Such an outcome is possible due to the vdW attraction.

4.4 Self-interstitials in graphite

Graphite is a common example of an extended vdW-bound material. Its structure consists of carbon layers that are held together by the dispersion interaction, while the intra-layer phenomena are determined by strong covalent bonds of sp^2-hybridised carbon atoms. The strength of these bonds is so enormous that formation of intrinsic defects, vacancies and interstitials, requires a relatively high energy. Specifically, the formation energy of a vacancy–interstitial pair known as Frenkel pair is 14 eV [60]. Upon recombination an energy of similar magnitude is released [61]. However, this process can be triggered at certain temperatures. Knowing details of such defect processes is important and an underappreciation of them can lead to serious consequences such as the fire accident in the Windscale nuclear reactor in 1957 [62].

A number of experimental studies on defects in graphite conducted in 1950–1960s contained measurements of annealed samples previously exposed to irradiation. It was found that the energy is released at various temperatures and the lowest one of them is 80 K [63, 60]. It was antic-

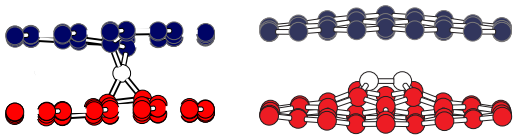

Figure 4.8. Energetically preferable structures of single interstitials (left) and di-interstitials (right). Atoms in the upper and lower layers as drawn in blue, red and white respectively.

ipated then that this particular energy release is triggered by diffusion of self-interstitials. These defects were pictured as free atoms confined between atomic layers of graphite. Since the interstitials were considered unbound, it was easy to relate them to the phenomena observed at 80 K – the temperature that corresponds to the energy barrier of ∼0.1–0.2 eV.

This model has become questioned after interstitials have been examined using DFT. It turned out that, in the energetically preferable structures (shown in Fig. 4.8), interstitials are covalently bound to either one or both adjacent carbon layers. Clearly, such interstitials cannot be mobile, since any type of a migration would require then bond breaking, which is energetically expensive and cannot occur at temperatures as low as 80 K. It was concluded then that the diffusion requires much higher temperatures and the low-temperature events potentially could be explained by different processes, for instance, local defect rearrangements and basal dislocation motion [61].

In Publication V, the question of the mobility of interstitials was readdressed, as the previous calculations provide just a fragmentary picture of the potential energy surface. Particularly, the experience accumulated in Publication IV shows that the knowledge of the energetic hierarchy of stationary structures is not sufficient. To build a sound model, it may be necessary to study also transition states of relevant structural transformations and previous papers do not contain an extensive study on these matters. Moreover, sometimes DFT calculations were compromised by the use of LDA, which is known to be especially inaccurate for chemical reactions [12]. Another popular method, GGA, somewhat improves the description of covalent bonds, but it misses another important aspect in graphite – the vdW interaction. In Publication V, the interstitial problem is considered using the vdW-DF method with the PBE exchange. Thus, a relatively high accuracy for chemical reactions is inherited from GGA without compromising the description of the vdW interactions. Structural transformations are examined by searching for transition states using the

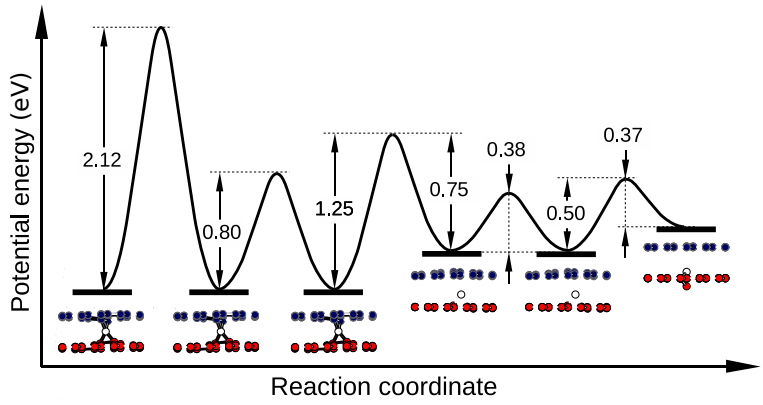

Figure 4.9. Schematic roadmap of structural transformations of single interstitials in bilayer graphene.

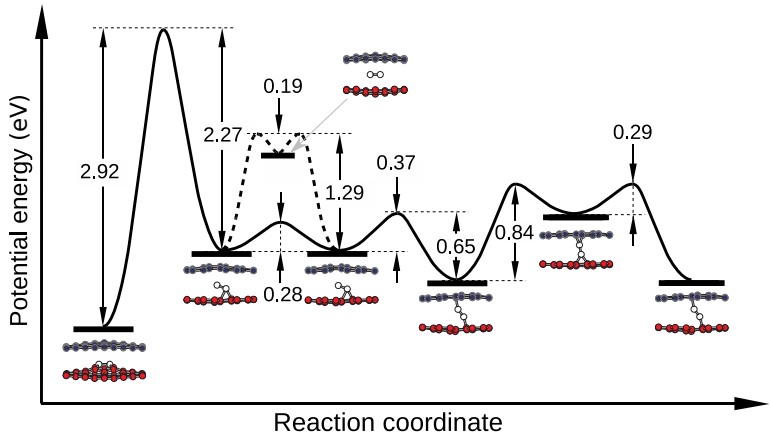

Figure 4.10. Schematic roadmap of structural transformations of di-interstitials in bilayer graphene.

nudged elastic band method combined with the dimer method [64, 65].

Due to computational limitations, structural transformations are considered only for interstitials in bilayer graphene. However, the obtained information can be generalised to bulk graphite as well. The results of calculations summarised in Figs. 4.9 and 4.10 show that the stable structures of single and di-interstitials are energywise well-separated from meta-stable structures. It means that samples irradiated at low enough temperatures contain different types of interstitials at the same time. For instance, annealing to the lowest single interstitial state requires the activation energy of 0.75 eV, which according to the Arrhenius equation (Eq. 4.1) corresponds to the transition time of 10^{34} s at the 80 K temperature!

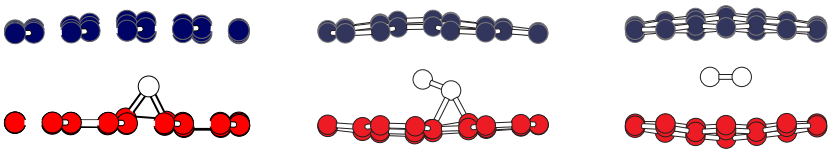

Figure 4.11. Structures of mobile interstitial species – grafted single interstitial (left), crane di-interstitial (centre) and free dimer di-interstitial (right).

The analysis of the meta-stable interstitial structures shows that a few of them are distinct from others by a low migration energy. Among the single interstitials, this property is observed for the grafted interstitial (see Fig. 4.11). For this interstitial the migration energy is 0.38 eV, which is 0.06 eV lower than that for an adatom on graphene. The difference reflects the presence of steric effects in the bi-layer case. In other words, a grafted interstitial takes a certain volume in the interlayer space and therefore repels one of the adjacent carbon layers (the blue one in Fig. 4.11). The equilibrium structure and energy are determined by a competition between this repulsion and the vdW attraction between the layers. This conclusion explains why it is important to describe the vdW interaction accurately even though the considered structural transformations are primarily related to cleavage and creation of covalent bonds.

The migration energy for the grafted interstitial has been obtained for a bilayer and should decrease for the bulk. Also, if zero-point vibration effects are considered, it decreases additionally by 0.07 eV. Combining these effects, the vdW-DF estimate for the interstitial migration energy is 0.3 eV that is comparable to the range of 0.1–0.2 eV anticipated from experiments.

The diffusion of the most mobile di-interstitial structures, the crane and the free dimer (see Fig. 4.11), requires the activation energies of 0.28 eV and 0.03 eV, respectively. The reason why the free dimer can migrate so easily is the absence of chemical bonds that would link it to the adjacent layers. An interstitial in this structure requires a little energy in order to resettle into a much more *comfortable* position and it is questionable how frequently can the free dimer occur directly upon irradiation. The same time, the crane di-interstitial can be produced by a reaction between two single interstitials and is also more likely to appear during irradiation.

In conclusion, the calculations in Publication V provide a comprehensive picture of structural transformations of interstitials. The results provide evidence that migration of interstitials can be responsible for the low-

temperature events observed in experiment. The reason why this was not previously deduced was the inability to recognise that bound (stable) and mobile (metastable) interstitials can coexist in a wide temperature range.

5. Summary

The van der Waals (vdW) interaction is an important and challenging issue in computational materials science. To resolve it, new methods emerge in the literature and one of the most prominent of them is the van der Waals density functional (vdW-DF). This approach introduces a truly non-local approximation to the correlation energy.

This Thesis is primarily devoted to an efficient implementation and versatile applications of the vdW-DF method. In Publication I, the adaptive real-space algorithm is introduced and applied for a benchmark set designed to study the performance of the method for intermolecular interactions. The calculations have revealed that the accuracy of the method varies with the choice of exchange, which is not strictly prescribed for the vdW-DF.

Publications II and III report on the application of the vdW-DF and the algorithm for a study of adsorption of flat organic molecules on two different surfaces. The accurate description of the vdW interaction allowed for explanation of the stability of the mobile molecules on the surfaces at room temperature. The mobility, in turn, leads to the formation of self-assembled structures, which are held together by weak hydrogen bonds that are influenced not only by electrostatic forces, but also by the dispersion.

Publication IV presents a detailed discussion of the adsorption of phenol on the Si(001)-(2$\times$1) surface. Although this study is concerned mainly with the dissociation of covalent bonds, the role of the vdW forces reveals itself at high coverages of the surface. The vdW attraction enables a high-density population of molecules on the surface, while methods that ignore this type of interaction predict a repulsive behaviour. This result potentially affects which of structures is observable after exposing the surface to the vapour.

Publication V contains a study on the questions of the relative stability and the mobility of self-interstitials in bulk graphite and bi-layer graphene. These defects introduce distortions in the layered structures of these materials, while the layers interact among themselves via vdW forces. Hence application of the vdW-DF allowed us to obtain credible energetics that predicts a coexistence of different types of interstitials at a wide range of temperatures. This result provides the evidence for the low-temperature diffusion of interstitials that is the simplest explanation of the low-temperature energy releases in annealing experiments.

More generally, this Thesis shows an example of how computational materials science advances due to evolving numerical algorithms rather than growing computing power. The efficient algorithm proposed here allowed for the study large-scale problems which would not have been tractable using the original implementation of vdW-DF. With this success in mind, I have a dream that one day many other sophisticated theories plagued by high numerical complexity will become accessible for a wide range of applications.

A. Kernel function in the vdW-DF

The kernel function introduced by Dion *et al.* in Ref. [24] is defined via the double integral

$$\varphi(d,d') = \frac{2}{\pi^2}\int_0^\infty \int_0^\infty a^2b^2W(a,b)T(v(a),v(b),v'(a),v'(b))dadb, \tag{A.1}$$

where

$$T(w,x,y,z) = \left[\frac{1}{w+x}+\frac{1}{y+z}\right]\left[\frac{1}{(w+y)(x+z)}+\frac{1}{(w+z)(x+y)}\right], \tag{A.2}$$

$$\begin{aligned} W(a,b) = [&(3-a^2)b\cos b\sin a + (3-b^2)a\cos a\sin b \\ &+(a^2+b^2-3)\sin b\sin a - 3ab\cos a\cos b]/(a^3b^3), \end{aligned} \tag{A.3}$$

$$v(a) = a^2/(2(1-e^{-\gamma a^2/d^2})) \tag{A.4}$$

and

$$v'(a) = a^2/(2(1-e^{-\gamma a^2/d'^2})). \tag{A.5}$$

Dimensionless variables $d = q_0(\mathbf{r})|\mathbf{r}-\mathbf{r}'|$ and $d' = q_0(\mathbf{r}')|\mathbf{r}-\mathbf{r}'|$, relate to D and δ used in Sec. 2.2.4 through linear relations $D = (d+d')/2$ and $\delta = (d-d')/(d+d')$. The kernel function is complicated and its frequent evaluation using Eqs. A.1–A.3 is unpractical. Instead, it is convenient to tabulate φ once and interpolate it whenever it has to be evaluated. Interpolation is discussed in Appendix B, while the rest of this Appendix is devoted to the numerical integration of Eq. A.1.

A careful inspection of the integrand $F(a,b) = a^2b^2W(a,b)T(a,b)$ reveals several length scale considerations. First, at large values of the variables, $F(a,b)$ decays as a power law that is scale-free, hence a quadrature on the whole semi-infinite interval has to be applied. $W(a,b)$ contains trigonometric functions with respect to both a and b. Second, it is important then to have a detailed enough quadrature grid for each oscillation period of 2π at least for meaningfully large values of the envelope function of the integrand. Finally, $T(a,b)$ contains two scales d and d' that appear

in the Gaussians of Eq. A.2. To summarise, $F(a,b)$ has a number of important scales, which are difficult to take into account at the same time and the validity of a direct application of the trapezoid rule and the Gauss quadratures is questionable. On the other hand, these difficulties can be taken care of automatically by adaptive integration routines available in the Quadpack library[66].

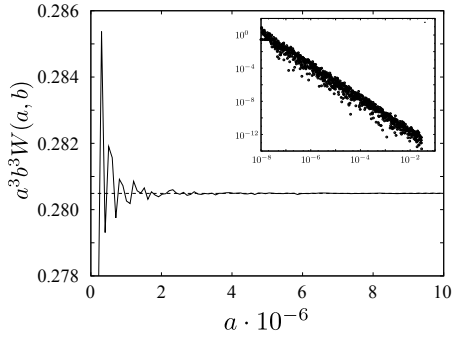

Figure A.1. Function $W(a, b = 1)$ computed directly using Eq. A.3 (solid line) and using the Taylor expansion at small a (dashed line). In both cases floating point operations are carried out in the double precision. The inset show the relative error of direct evaluation of the function at different values of a.

The large-d and d' asymptotics of the kernel function is well-known [24] and the numerical integration procedure described here accurately recovers it. On the other hand, the small-d and d' behaviour has been derived and is scarcely mentioned in Ref. [67]. This is understandable, since the integrand of Eq. A.1 has important features in the both ranges $0 < a, b < d, d'$ and $0 < a, b < \infty$. The problem becomes even more tricky due to the numerical noise produced by the round-off errors in $W(a,b)$. As shown in Fig. A.1, the direct evaluation of $W(a,b)$ is severely compromised at small values of a and/or b. In order to avoid the round-off errors, $W(a,b)$ is Taylor-expanded in the problematic region. It allows to calculate the kernel function accurately and to reveal its asymptotic behaviour, which is shown in Fig. A.2. At small values of d and d'(or equivalently at small values of D),

$$\varphi(D,\delta) \sim \alpha(\delta) - \beta \ln(D), \tag{A.6}$$

where $\alpha(\delta)$ is some function and β is a constant. According to numerical calculations β coincides with $2/\pi$ up to seventh sign for each considered δ.

The obtained asymptotic form of the kernel function agrees well with the findings of Vydrov and Voorhis [67] and contradicts the graph of the derivative of the kernel function acquired by Thonhauser *et al.* in Ref.[68].

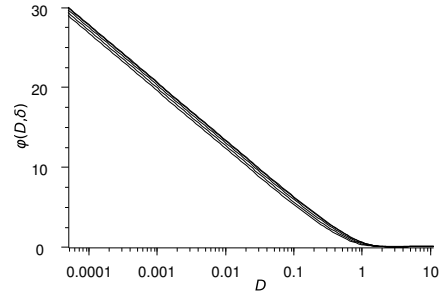

Figure A.2. Small D asymptotics of the vdW-DF kernel function at represented as a family of lines corresponding to the range $0 \leq \delta \leq 1$.

Tests, however, show that, if an algorithm for evaluating Eq. 2.9 can handle the behaviour of the kernel function at $D = 0$, the logarithmic singularity itself has an insignificant role in real systems. Then, it is justifiable to store a table of $D^2\varphi(D, \delta)$ values without extra resolution for small D. This observation has a practical meaning, as the look-up table can be rather compact.

B. Interpolation

The algorithm described in Sec. 3 requires an efficient procedure to evaluate the density $n(\mathbf{r})$ at any given $\mathbf{r}$. A calculation via one-electron orbitals using basis functions is too slow and hence inappropriate regardless of the type of the basis. Instead, it turns out to be much more practical to interpolate charge densities precomputed on evenly-spaced grids. Electronic structure codes such as SIESTA and VASP employ either pseudopotentials or projector-augmented waves and deal with smooth pseudodensities. It means that even a low-order polynomial interpolation can be suitable for these purposes.

The simplest and fastest approach is the (tri-)linear interpolation. If the function $f(x)$ is known at the ends of the unity interval $[0;1]$, it can be approximated as $f(x) \approx (1-x)f(0) + xf(1)$. Rewritten in a more compact manner

$$f(x) \approx \sum_{i\in\{0;1\}} A_i^{(x)} f_i, \tag{B.1}$$

with $A_0^{(x)} = 1-x$, $A_1^{(x)} = x$ and $f_i = f(i)$. The uni-variate linear interpolation is trivial to generalise to the tri-variate case

$$f(x,y,z) \approx \sum_{i,j,k\in\{0;1\}} A_i^{(x)} A_j^{(y)} A_k^{(z)} f_{ijk}. \tag{B.2}$$

Such an approximation is easy to implement and fast to run. Unfortunately, the linear interpolation converges too slowly with respect to the grid resolution. It also yields a continuous, but not smooth a function that makes the linear interpolation useless if continuous derivatives are also required. For the same reason, the Lagrange polynomial interpolation is not suitable either.

Nevertheless, the smoothness of an interpolating function can be easily arranged in one dimension. Assume, the second derivative f_i'' is tabulated at grid points. Then, $f''(x)$ can be approximated by a piecewise linear

function or, specifically for the unity interval, as

$$f''(x) \approx (1-x)f_0'' + xf_1''. \tag{B.3}$$

The double integration of Eq. B.3 and the knowledge of the function values at the endpoints of the interval leads to

$$f(x) \approx (1-x)f_0 + xf_1 + \frac{(1-x)^3-(1-x)}{6}f_0'' + \frac{x^3-x}{6}f_1'' \tag{B.4}$$

and

$$f'(x) \approx -f_0 + f_1 - \frac{3(1-x)^2-1}{6}f_0'' + \frac{3x^2-1}{6}f_1''. \tag{B.5}$$

The same result rewritten in a more compact form reads as

$$f(x) \approx \sum_{i\in\{0;1\}} \left(A_i^{(x)} f_i + B_i^{(x)} f_i''\right) \tag{B.6}$$

and

$$f'(x) \approx \sum_{i\in\{0;1\}} (-1)^{i+1} \left(f_i + C_i^{(x)} f_i''\right), \tag{B.7}$$

where $B_i^{(x)} = ((A_i^{(x)})^3 - A_i^{(x)})/6$ and $C_i^{(x)} = (3(A_i^{(x)})^2 - 1)/6$. Eqs. B.5 and B.7 show that the smoothness of $f(x)$ at the endpoints of intervals restricts f_i''. In practice, the second derivative is not given in advance and has to be computed following the restrictions. As explained in Ref. [69], a calculation of f_i'' requires solving a tridiagonal linear set of equations with the number of unknowns equal to the number of tabulated function values. This effort scales as $O(N)$, but it has to be faced just once at the initialisation phase and the computational complexity of each interpolation event is $O(1)$.

The most straightforward generalisation of the cubic spline interpolation to the multi-variate case is described in Ref. [69]. The idea is to apply the uni-variate interpolation for each dimension, but this approach is very expensive and hence is not suitable for heavy-duty applications. Instead, it is possible to follow a different strategy that also allows to obtain smooth interpolation, but with a considerably smaller effort. Consider an evenly spaced structured $N_x \times N_y$ grid, on which the function $f(x,y)$ is tabulated. Similarly to Eq. B.3, the function can be approximated

$$f_{xx}''(x,y) \approx \sum_{i,j\in\{0;1\}} A_i^{(x)} A_j^{(y)} f_{xx}''(x_i,y_j) \tag{B.8}$$

and

$$f_{yy}''(x,y) \approx \sum_{i,j\in\{0;1\}} A_i^{(x)} A_j^{(y)} f_{yy}''(x_i,y_j). \tag{B.9}$$

Double integration of these expressions and inserting boundary conditions lead to the spline interpolation formula

$$\begin{aligned} f(x,y) \approx \sum_{i,j\in\{0;1\}} [&A_i^{(x)} A_j^{(y)} f(x_i,y_j) \\ &+ B_i^{(x)} A_j^{(y)} f''_{xx}(x_i,y_j) \\ &+ A_i^{(x)} B_j^{(y)} f''_{yy}(x_i,y_j)]. \end{aligned} \tag{B.10}$$

The result does not contain cross-derivatives, which means that a calculation of $f''_{xx}(x_i,y_j)$ and $f''_{yy}(x_i,y_j)$ can be carried out separately for every grid line along x and y. The effort to obtain all values of $f''_{xx}(x_i,y_j)$ and $f''_{yy}(x_i,y_j)$ scales as $O(N_xN_y)$ and it has to be faced once during the initialisation. An evaluation of $f(x,y)$ requires $O(1)$ operations although it is more expensive than in the uni-variate case.

This approach is not equivalent to the bicubic spline interpolation described in Ref. [69] neither effort-wise nor mathematically. The bicubic spline polynomial of Ref. [69] contains x^iy^j with $i,j \in \{0,1,2,3\}$ – 16 terms altogether, while Eq. B.10 contains only 12 of them, specifically, 1, x, y, xy, x^2, x^3, x^2y, x^3y, y^2, y^3, xy^2, xy^3. Yet, it proved very useful in practical applications. A generalisation to the tri-variate case contains 32 terms instead of 64 in a tricubic polynomial and it reads as

$$\begin{aligned} f(x,y,z) \approx \sum_{i,j,k\in\{0;1\}} [&A_i^{(x)} A_j^{(y)} A_k^{(z)} f(x_i,y_j,z_k) \\ &+ B_i^{(x)} A_j^{(y)} A_k^{(z)} f''_{xx}(x_i,y_j,z_k) \\ &+ A_i^{(x)} B_j^{(y)} A_k^{(z)} f''_{yy}(x_i,y_j,z_k) \\ &+ A_i^{(x)} A_j^{(y)} B_k^{(z)} f''_{zz}(x_i,y_j,z_k)]. \end{aligned} \tag{B.11}$$

C. Adaptive quadrature grids

The linear scaling of the adaptive real-space algorithm described in Sec. 3.2 makes it affordable for large applications, where the time spent on evaluating $E_{\mathrm{c}}^{\mathrm{nl}}$, $\varepsilon_{\mathrm{c}}^{\mathrm{nl}}(\mathrm{r})$ and $v_{\mathrm{c}}^{\mathrm{nl}}(\mathrm{r})$ is just a small fraction of the entire DFT calculation. For smaller systems this is not the case and a vdW-DF calculation can be several times more expensive than a GGA calculation for the same system. The situation can be improved by varying the effort spent on each point, where the correlation energy density and potential has to be evaluated. For example, if at some point $\mathbf{r}$ the electron density is very small, say, smaller than some n_{thr}, the energy density and the potential can be set to zero without any harm to the overall accuracy. But it may occur that $n_{\mathrm{thr}} < n(\mathbf{r}) < 10n_{\mathrm{thr}}$, what to do then? The energy density cannot be disregarded at such a point. On the other hand, it is clear that evaluation of $\varepsilon_{\mathrm{c}}^{\mathrm{nl}}(\mathbf{r})$ may be less accurate than if $n(\mathbf{r})$ were ten times higher. Such an example shows that computational expenses can be reduced if the size of quadrature grid, namely, the number of radial shells and the order of Lebedev's quadrature are adjusted according to local accuracy requirements. In practice, the number of radial shells N_{rad} is selected according to

$$N_{\mathrm{rad}} = \max\{N_0 + k \ln \frac{n(\mathbf{r})}{n_0}, N_0\}, \tag{C.1}$$

where $n_0 = 1\ a_0^{-3}$, but N_0 and k are empirically chosen parameters.

The effort spent on the angular integral over a sphere can be reduced if the radius of the sphere and the distance between the grid points are small, since the densities used in practical calculations are so smooth that they can be accurately approximated by low-order polynomials. Contributions of high spherical harmonics are low in this case and the necessary size of the angular grid can be estimated as

$$N_{\mathrm{ang}} \geq \frac{R^2}{R_0^2}, \tag{C.2}$$

where R is the radius of a spherical shell and R_0 is an empirical parameter.

D. Accuracy benchmarks

To validate the implementation of the adaptive real-space approach in the VASP code, test calculations are performed and compared to the results of Ref. [70]. The authors of that paper use their own real-space algorithm embedded in an all-electron code and their own table of the kernel function. In other words, these two implementations are completely indepent. The results of the test calculations are summarised in Fig. D.1, which contains the interaction energy curves for the argon and methane dimers as well as for the methane-benzene complex.

For all of the three studied complexes, the data obtained in the present efforts and in Ref. [70] agree well, but do not coincide. The anticipated source of discrepancies is the use of the pseudo-valence electron densities in the present Thesis in contrast to the all-electron densities in Ref. [70].

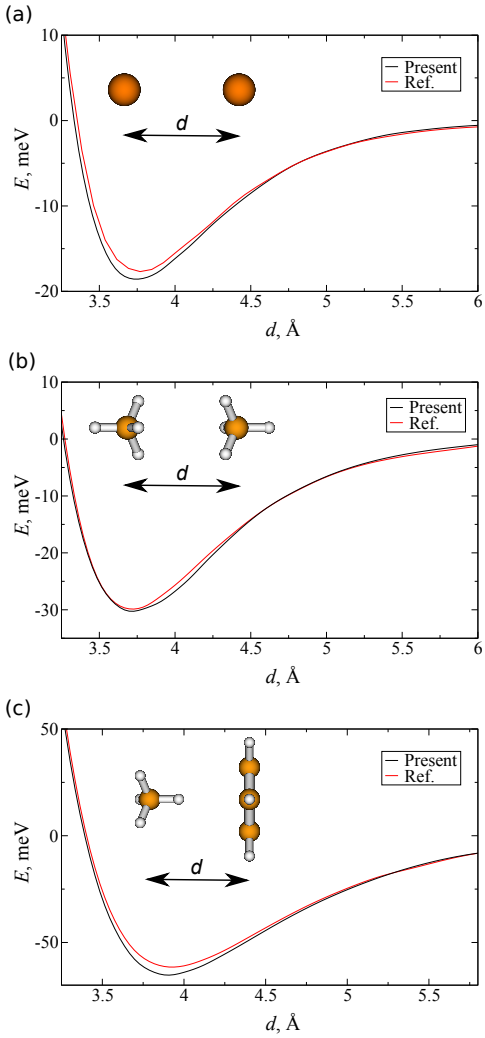

Figure D.1. vdW-DF2 [28] interaction energy curves for (a) argon dimer, (b) methane dimer and (c) methane-benzene complex. Data from Ref. [70] are shown for a reference. The separation distances d and geometries of monomers are defined consistently with Ref. [71].

E. Self-consistency and forces

The first self-consistent vdW-DF calculations have been reported a couple of years after the vdW-DF method was published [68]. Until then the method was applied non-self-consistently (perturbatively) for a number of applications. In fact, it is still applied as a post-correction if the $E_{\mathrm{c}}^{\mathrm{nl}}$ integration routine is implemented using the expensive brute-force algorithm, because obtaining self-consistency requires recalculating of $\epsilon_{\mathrm{c}}^{\mathrm{nl}}(\mathbf{r})$ and $v_{\mathrm{c}}^{\mathrm{nl}}(\mathbf{r})$ several times. It makes the brute-force algorithm even more expensive. With the emergence of faster integration algorithms, obtaining self-consistent Kohn-Sham orbitals does not require an enormous effort anymore and there is no reason for performing vdW-DF calculations non-self-consistently.

The exchange-correlation potential, which is a part of the effective potential in the Kohn-Sham equations, is defined as

$$v_{\mathrm{xc}}(\mathbf{r}) = \frac{\delta E_{\mathrm{xc}}\left[n(\mathbf{r})\right]}{\delta n(\mathbf{r})}. \tag{E.1}$$

In practice, when GGA is used, it is expressed as

$$v_{\mathrm{xc}} = \frac{\partial(n\epsilon_{\mathrm{xc}})}{\partial n} - \nabla\frac{\partial(n\epsilon_{\mathrm{xc}})}{\partial(\nabla n)} \tag{E.2}$$

or, equivalently,

$$v_{\mathrm{xc}} = \epsilon_{\mathrm{xc}} + n\frac{\partial(\epsilon_{\mathrm{xc}})}{\partial n} - \nabla\frac{\partial(n\epsilon_{\mathrm{xc}})}{\partial(\nabla n)}. \tag{E.3}$$

For instance, in the DFT codes SIESTA and VASP, the energy density ϵ_{xc} and the derivatives $\partial\epsilon_{\mathrm{xc}}/\partial n$ and $\partial\epsilon_{\mathrm{xc}}/\partial(\nabla n)$ (or $\partial\epsilon_{\mathrm{xc}}/\partial|\nabla n|$) are evaluated, and then they are combined together to obtain the potential. This means that if $v_{\mathrm{c}}^{\mathrm{nl}}$ could be presented in the form of Eq. E.3, a self-consistent implementation of the vdW-DF can exploit the already existing infrastructure of the two codes.

To derive $v_{\mathrm{c}}^{\mathrm{nl}}$, it is convenient to write $E_{\mathrm{c}}^{\mathrm{nl}} = E_{\mathrm{c}}^{\mathrm{nl}}\left[n(\mathbf{r_1}), n(\mathbf{r_2})\right]$. Then, the potential is still evaluated as $v_{\mathrm{c}}^{\mathrm{nl}}(\mathbf{r}) = \delta E_{\mathrm{c}}^{\mathrm{nl}}\left[n(\mathbf{r_1}), n(\mathbf{r_2})\right]/\delta n(\mathbf{r})$, but one has

to keep in mind relation

$$\partial f(\mathbf{r_1})/\partial n(\mathbf{r}) = \delta(\mathbf{r}-\mathbf{r_1})\partial f(\mathbf{r})/\partial n(\mathbf{r}). \tag{E.4}$$

Inserting Eq. 2.9 into Eq. E.3 yields

$$\begin{aligned} v_{\mathrm{c}}^{\mathrm{nl}}(\mathbf{r}) = & \frac{1}{2}\iint \frac{\partial n(\mathbf{r_1})}{\partial n(\mathbf{r})}\varphi(\mathbf{r_1},\mathbf{r_2})n(\mathbf{r_2})d^3r_1d^3r_2 \\ & + \frac{1}{2}\iint n(\mathbf{r_1})\varphi(\mathbf{r_1},\mathbf{r_2})\frac{\partial n(\mathbf{r_2})}{\partial n(\mathbf{r})}d^3r_1d^3r_2 \\ & + \frac{1}{2}\iint n(\mathbf{r_1})\frac{\partial\varphi(\mathbf{r_1},\mathbf{r_2})}{\partial n(\mathbf{r})}n(\mathbf{r_2})d^3r_1d^3r_2 \\ & - \frac{1}{2}\nabla\left(\iint n(\mathbf{r_1})\frac{\partial\varphi(\mathbf{r_1},\mathbf{r_2})}{\partial(\nabla n(\mathbf{r}))}n(\mathbf{r_2})d^3r_1d^3r_2\right), \end{aligned} \tag{E.5}$$

where the sum of the first two terms transforms into $2\epsilon_{\mathrm{c}}^{\mathrm{nl}}$ after Eq. E.4 is applied. The derivative from the third term can be rewritten using the chain-rule

$$\begin{aligned} \frac{\partial\varphi(D(\mathbf{r_1},\mathbf{r_2}),\Delta(\mathbf{r_1},\mathbf{r_2}))}{\partial n(\mathbf{r})} = & \\ & \frac{\partial\varphi(D(\mathbf{r_1},\mathbf{r_2}),\Delta(\mathbf{r_1},\mathbf{r_2}))}{\partial D(\mathbf{r_1},\mathbf{r_2})}\frac{\partial D(\mathbf{r_1},\mathbf{r_2})}{\partial q_0(\mathbf{r})}\frac{\partial q_0(\mathbf{r})}{\partial n(\mathbf{r})} \\ & + \frac{\partial\varphi(D(\mathbf{r_1},\mathbf{r_2}),\Delta(\mathbf{r_1},\mathbf{r_2}))}{\partial\Delta(\mathbf{r_1},\mathbf{r_2})}\frac{\partial\Delta(\mathbf{r_1},\mathbf{r_2})}{\partial q_0(\mathbf{r})}\frac{\partial q_0(\mathbf{r})}{\partial n(\mathbf{r})}, \end{aligned} \tag{E.6}$$

where

$$D(\mathbf{r_1},\mathbf{r_2}) = \frac{q_0(\mathbf{r_1})+q_0(\mathbf{r_2})}{2}|\mathbf{r_2}-\mathbf{r_1}| \tag{E.7}$$

and

$$\Delta(\mathbf{r_1},\mathbf{r_2}) = \frac{q_0(\mathbf{r_1})-q_0(\mathbf{r_2})}{q_0(\mathbf{r_1})+q_0(\mathbf{r_2})}. \tag{E.8}$$

The derivatives $\partial\varphi/\partial D$ and $\partial\varphi/\partial\Delta$, in principle, are known. More specifically, they can be stored in separate tables or can be computed from the φ-table using the spline interpolation in the manner described in Appendix B. The other derivative, $\partial q_0(\mathbf{r})/\partial n(\mathbf{r})$, is straightforward to obtain from Eq. 2.11. Finally, using Eqs. E.4, E.7 and E.8, the remaining multipliers of Eq. E.6 are obtained as

$$\frac{\partial D(\mathbf{r_1},\mathbf{r_2})}{\partial q_0(\mathbf{r})} = \frac{\delta(\mathbf{r}-\mathbf{r_1})+\delta(\mathbf{r}-\mathbf{r_2})}{2}|\mathbf{r_1}-\mathbf{r_2}|, \tag{E.9}$$

$$\frac{\partial\Delta(\mathbf{r_1},\mathbf{r_2})}{\partial q_0(\mathbf{r})} = \frac{2(q_0(\mathbf{r_2})\delta(\mathbf{r}-\mathbf{r_1})+q_0(\mathbf{r_1})\delta(\mathbf{r}-\mathbf{r_2}))}{(q_0(\mathbf{r_2})+q_0(\mathbf{r_1}))^2}. \tag{E.10}$$

To derive the last summand in Eq. E.5, it is necessary to repeat the steps done in Eqs. E.6–E.10 with the only difference that $\partial q_0/\partial n$ is replaced by

$\partial q_0/\partial(\nabla n)$. The integration of the obtained expression leads to the final answer

$$\begin{aligned} v_{\mathrm{c}}^{\mathrm{nl}}(\mathbf{r}) &= 2\epsilon_{\mathrm{c}}^{\mathrm{nl}}(\mathbf{r}) \\ &+ \frac{1}{2}\left(n(\mathbf{r})\frac{\partial q_0(\mathbf{r})}{\partial n(\mathbf{r})} - \nabla\left(n(\mathbf{r})\frac{\partial q_0(\mathbf{r})}{\partial \nabla n(\mathbf{r})}\right) - n(\mathbf{r})\frac{\partial q_0(\mathbf{r})}{\partial \nabla n(\mathbf{r})}\nabla\right) \\ &\times \int \left(\frac{\partial \varphi}{\partial D}\left|\mathbf{r}-\mathbf{r}'\right| + \frac{\partial \varphi}{\partial \Delta}\frac{4q_0(\mathbf{r}')}{(q_0(\mathbf{r})+q_0(\mathbf{r}'))^2}\right) d^3r'. \end{aligned} \tag{E.11}$$

A careful inspection of the obtained expression for $v_{\mathrm{c}}^{\mathrm{nl}}$ shows that it has the same form as Eq. E.3, which is the desired result. From the technical point of view, Eqs. E.3 and 3.2 contain the same kind of integrals and an evaluation of $\partial\epsilon_{\mathrm{xc}}/\partial n$ and $\partial\epsilon_{\mathrm{xc}}/\partial(\nabla n)$ required for obtaining $v_{\mathrm{c}}^{\mathrm{nl}}(\mathbf{r})$ does not require any different numerical approach than that for $\epsilon_{\mathrm{c}}^{\mathrm{nl}}(\mathbf{r})$. In practice, integrals of all the three terms are evaluated on a same quadrature grid using the adaptive real-space approach.

The capability to evaluate the potential actually brings more than just a self-consistent solution and a confidence of having a better justified total energy. In a number of codes, including VASP and SIESTA, this capability translates into the availability of Hellmann-Feynman forces [44, 43]. It opens a road for a large number of applications that require a non-trivial study of the potential energy surface ranging from a ionic relaxation to a search for transition states relevant for diffusion and chemical reactions.

Bibliography

[1] Michael E. Harding, Juana Vázquez, Branko Ruscic, Angela K. Wilson, Jürgen Gauss, and John F. Stanton. High-accuracy extrapolated ab initio thermochemistry. III. Additional improvements and overview. *The Journal of Chemical Physics*, 128(11):114111, 2008.

[2] Ralf Peter Stoffel, Claudia Wessel, Marck-Willem Lumey, and Richard Dronskowski. Ab Initio Thermochemistry of Solid-State Materials. *Angewandte Chemie International Edition*, 49(31):5242–5266, 2010.

[3] P. Hohenberg and W. Kohn. Inhomogeneous Electron Gas. *Phys. Rev.*, 136(3B):B864–B871, 1964.

[4] W. Kohn and L. J. Sham. Self-Consistent Equations Including Exchange and Correlation Effects. *Phys. Rev.*, 140(4A):A1133–A1138, 1965.

[5] O. Gunnarsson and B. I. Lundqvist. Exchange and correlation in atoms, molecules, and solids by the spin-density-functional formalism. *Phys. Rev. B*, 13(10):4274–4298, 1976.

[6] David C. Langreth and John P. Perdew. Exchange-correlation energy of a metallic surface: Wave-vector analysis. *Phys. Rev. B*, 15(6):2884–2901, 1977.

[7] H. C. Longuet-Higgins. Spiers Memorial Lecture: Intermolecular forces. *Discuss. Faraday Soc.*, 40:7–18, 1965.

[8] E. Zaremba and W. Kohn. Van der Waals interaction between an atom and a solid surface. *Phys. Rev. B*, 13(6):2270–2285, 1976.

[9] Attila Szabo and Neil S. Ostlund. *Modern Quantum Chemistry: Introduction to Advanced Electronic Structure Theory*. Dover Publications, 1996.

[10] Petr Jurečka, Jiří Šponer, Jiří Černý, and Pavel Hobza. Benchmark database of accurate (MP2 and CCSD(T) complete basis set limit) interaction energies of small model complexes, DNA base pairs, and amino acid pairs. *Phys. Chem. Chem. Phys.*, 8(17):1985 – 1993, 2006.

[11] J Cizek and J Paldus. Coupled Cluster Approach. *Physica Scripta*, 21(3-4):251, 1980.

[12] Jingjing Zheng, Yan Zhao, and Donald G. Truhlar. Representative Benchmark Suites for Barrier Heights of Diverse Reaction Types and Assessment of Electronic Structure Methods for Thermochemical Kinetics. *Journal of Chemical Theory and Computation*, 3(2):569–582, 2007.

[13] D. C. Langreth, B I Lundqvist, S D Chakarova-Kack, V R Cooper, M Dion, P Hyldgaard, A Kelkkanen, J Kleis, Lingzhu Kong, Shen Li, P G Moses, E Murray, A Puzder, H Rydberg, Schroder E, and Thonhauser T. A density functional for sparse matter. *J. Phys.: Condens. Matter*, 21(8):084203, 2009.

[14] John F. Dobson, Keith McLennan, Angel Rubio, Jun Wang, Tim Gould, Hung M. Le, and Bradley P. Dinte. Prediction of Dispersion Forces: Is There a Problem? *Australian Journal of Chemistry*, 54:513–527, 2001.

[15] Stefan Grimme. Accurate description of van der Waals complexes by density functional theory including empirical corrections. *J. Comput. Chem.*, 25(12):1463–1473, 2004.

[16] Stefan Grimme. Semiempirical GGA-type density functional constructed with a long-range dispersion correction. *Journal of Computational Chemistry*, 27(15):1787–1799, 2006.

[17] Stefan Grimme, Jens Antony, Stephan Ehrlich, and Helge Krieg. A consistent and accurate ab initio parametrization of density functional dispersion correction (DFT-D) for the 94 elements H-Pu. 132(15):154104, 2010.

[18] Alexandre Tkatchenko and Matthias Scheffler. Accurate Molecular Van Der Waals Interactions from Ground-State Electron Density and Free-Atom Reference Data. *Phys. Rev. Lett.*, 102:073005, Feb 2009.

[19] Axel D. Becke and Erin R. Johnson. Exchange-hole dipole moment and the dispersion interaction. *The Journal of Chemical Physics*, 122(15):154104, 2005.

[20] Axel D. Becke and Erin R. Johnson. A density-functional model of the dispersion interaction. *The Journal of Chemical Physics*, 123(15):154101, 2005.

[21] John F. Dobson, Angela White, and Angel Rubio. Asymptotics of the Dispersion Interaction: Analytic Benchmarks for van der Waals Energy Functionals. *Phys. Rev. Lett.*, 96(7):073201, Feb 2006.

[22] S. Lebègue, J. Harl, Tim Gould, J. G. Ángyán, G. Kresse, and J. F. Dobson. Cohesive Properties and Asymptotics of the Dispersion Interaction in Graphite by the Random Phase Approximation. *Phys. Rev. Lett.*, 105(19):196401, Nov 2010.

[23] Felix Hanke. Sensitivity analysis and uncertainty calculation for dispersion corrected density functional theory. *Journal of Computational Chemistry*, 32(7):1424–1430, 2011.

[24] M. Dion, H. Rydberg, E. Schröder, D. C. Langreth, and B. I. Lundqvist. Van der Waals Density Functional for General Geometries. *Phys. Rev. Lett.*, 92(24):246401, 2004.

[25] Oleg A. Vydrov and Troy Van Voorhis. Improving the accuracy of the nonlocal van der Waals density functional with minimal empiricism. *The Journal of Chemical Physics*, 130(10):104105, 2009.

[26] David C. Langreth and S.H. Vosko. Response Functions and Nonlocal Approximations. In Per-Olov Löwdin, editor, *Density Functional Theory of Many-Fermion Systems*, volume 21 of *Advances in Quantum Chemistry*, pages 175 – 199. Academic Press, 1990.

[27] Peter Elliott and Kieron Burke. Non-empirical derivation of the parameter in the B88 exchange functional. *Canadian Journal of Chemistry*, 87(10):1485–1491, 2009.

[28] Kyuho Lee, Éamonn D. Murray, Lingzhu Kong, Bengt I. Lundqvist, and David C. Langreth. Higher-accuracy van der Waals density functional. *Phys. Rev. B*, 82(8):081101, 2010.

[29] Oleg A. Vydrov and Troy Van Voorhis. Nonlocal Van der Waals Density Functionals Based on Local Response Models. In Miguel A.L. Marques, Neepa T. Maitra, Fernando Manuel da Silva Nogueira, E.K.U. Gross, and Angel Rubio, editors, *Fundamentals of Time-Dependent Density Functional Theory*, volume 837 of *Lecture Notes in Physics*. Springer, Berlin, 2012. Preprint http://www.mit.edu/∼vydrov/vdW-Chapter.pdf.

[30] Yingkai Zhang and Weitao Yang. Comment on Generalized Gradient Approximation Made Simple. *Phys. Rev. Lett.*, 80(4):890, 1998.

[31] Andris Gulans, Martti J. Puska, and Risto M. Nieminen. Linear-scaling self-consistent implementation of the van der Waals density functional. *Phys. Rev. B*, 79(20):201105, 2009.

[32] Guillermo Román-Pérez and José M. Soler. Efficient Implementation of a van der Waals Density Functional: Application to Double-Wall Carbon Nanotubes. *Phys. Rev. Lett.*, 103(9):096102, 2009.

[33] Dmitrii Nabok, Peter Puschnig, and Claudia Ambrosch-Draxl. noloco: An efficient implementation of van der Waals density functionals based on a Monte-Carlo integration technique. *Computer Physics Communications*, 182(8):1657 – 1662, 2011.

[34] A. D. Becke. A multicenter numerical integration scheme for polyatomic molecules. *J. Chem. Phys.*, 88(4):2547–2553, 1988.

[35] V. I. Lebedev. Values of the nodes and weights of quadrature formulas of Gauss-Markov type for a sphere from the ninth to seventeenth order of accuracy that are invariant with respect to an octahedron group with inversion. *Zh. Vychisl. Mat. Mat. Fiz.*, 15:48–54, 1975.

[36] V. I. Lebedev. Quadratures on the sphere. *Zh. Vychisl. Mat. Mat. Fiz.*, 16(2):293–306, 1976.

[37] Christopher W. Murray, Nicholas C. Handy, and Gregory J. Laming. Quadrature schemes for integrals of density functional theory. *Molecular Physics*, 78(4):997–1014, 1993.

[38] Peter M. W. Gill, Benny G. Johnson, and John A. Pople. A standard grid for density functional calculations. *Chemical Physics Letters*, 209(5-6):506 – 512, 1993.

[39] Jonas Björk, Felix Hanke, Carlos-Andres Palma, Paolo Samori, Marco Cecchini, and Mats Persson. Adsorption of Aromatic and Anti-Aromatic Systems on Graphene through π-π Stacking. *The Journal of Physical Chemistry Letters*, 1(23):3407–3412, 2010.

[40] Philip Donovan, Abel Robin, Matthew S. Dyer, Mats Persson, and Rasmita Raval. Unexpected Deformations Induced by Surface Interaction and Chiral Self-Assembly of CoII-Tetraphenylporphyrin (Co-TPP) Adsorbed on Cu(110): A Combined STM and Periodic DFT Study. *Chemistry – A European Journal*, 16(38):11641–11652, 2010.

[41] Karen Johnston, Andris Gulans, Tuukka Verho, and Martti J. Puska. Adsorption structures of phenol on the Si(001)-(2×1) surface calculated using density functional theory. *Phys. Rev. B*, 81(23):235428, 2010.

[42] Piotr T. Czekala, Haiping Lin, Werner A. Hofer, and Andris Gulans. Acetylene adsorption on silicon (100)-(4×2) revisited. *Surface Science*, 605(15-16):1341 – 1346, 2011.

[43] Pablo Ordejón, Emilio Artacho, and José M. Soler. Self-consistent order-N density-functional calculations for very large systems. *Phys. Rev. B*, 53(16):R10441–R10444, 1996.

[44] G. Kresse and J. Furthmüller. Efficient iterative schemes for ab initio total-energy calculations using a plane-wave basis set. *Phys. Rev. B*, 54:11169–11186, 1996.

[45] O. H. Pakarinen, J. M. Mativetsky, A. Gulans, M. J. Puska, A. S. Foster, and P. Grutter. Role of van der Waals forces in the adsorption and diffusion of organic molecules on an insulating surface. *Phys. Rev. B*, 80(8):085401, 2009.

[46] M. Mura, A. Gulans, T. Thonhauser, and L. Kantorovich. Role of van der Waals interaction in forming molecule-metal junctions: flat organic molecules on the Au(111) surface. *Phys. Chem. Chem. Phys.*, 12:4759–4767, 2010.

[47] M. Mura, X. Sun, F. Silly, H. T. Jonkman, G. A. D. Briggs, M. R. Castell, and L. N. Kantorovich. Experimental and theoretical analysis of H-bonded supramolecular assemblies of PTCDA molecules. *Phys. Rev. B*, 81(19):195412, 2010.

[48] Andris Gulans, Arkady V. Krasheninnikov, Martti J. Puska, and Risto M. Nieminen. Bound and free self-interstitial defects in graphite and bilayer graphene: A computational study. *Phys. Rev. B*, 84(2):024114, 2011.

[49] Karen Johnston and Vagelis Harmandaris. Properties of Benzene Confined between Two Au(111) Surfaces Using a Combined Density Functional Theory and Classical Molecular Dynamics Approach. *The Journal of Physical Chemistry C*, 115(30):14707–14717, 2011.

[50] Florian Göltl and Jürgen Hafner. Alkane adsorption in Na-exchanged chabazite: The influence of dispersion forces. *The Journal of Chemical Physics*, 134(6):064102, 2011.

[51] Jonas Björk, Sven Stafström, and Felix Hanke. Zipping Up: Cooperativity Drives the Synthesis of Graphene Nanoribbons. *Journal of the American Chemical Society*, 133(38):14884–14887, 2011.

[52] John P. Perdew, Kieron Burke, and Matthias Ernzerhof. Generalized Gradient Approximation Made Simple. *Phys. Rev. Lett.*, 77(18):3865, 1996.

[53] Fabien Silly, Adam Q. Shaw, Martin R. Castell, G. A. D. Briggs, Manuela Mura, Natalia Martsinovich, and Lev Kantorovich. Melamine Structures on the Au(111) Surface. *The Journal of Physical Chemistry C*, 112(30):11476–11480, 2008.

[54] Gautam R. Desiraju. Hydrogen Bridges in Crystal Engineering: Interactions without Borders. *Accounts of Chemical Research*, 35(7):565–573, 2002.

[55] Karen Johnston, Jesper Kleis, Bengt I. Lundqvist, and Risto M. Nieminen. Influence of van der Waals forces on the adsorption structure of benzene on silicon studied using density functional theory. *Phys. Rev. B*, 77(12):121404, 2008.

[56] M.P. Casaletto, M. Carbone, M.N. Piancastelli, K. Horn, K. Weiss, and R. Zanoni. A high resolution photoemission study of phenol adsorption on Si(100)2×1. *Surface Science*, 582(1-3):42 – 48, 2005.

[57] J. P. Perdew. *Electronic Structure of Solids '91*. Akademie Verlag, Berlin, 1991.

[58] P. J. Stephens, F. J. Devlin, C. F. Chabalowski, and M. J. Frisch. Ab Initio Calculation of Vibrational Absorption and Circular Dichroism Spectra Using Density Functional Force Fields. *The Journal of Physical Chemistry*, 98(45):11623–11627, 1994.

[59] P. Maragakis, Stefan A. Andreev, Yisroel Brumer, David R. Reichman, and Efthimios Kaxiras. Adaptive nudged elastic band approach for transition state calculation. *The Journal of Chemical Physics*, 117(10):4651–4658, 2002.

[60] P. A. Thrower and R. M. Mayer. Point defects and self-diffusion in graphite. *physica status solidi (a)*, 47(1):11, 1978.

[61] R. H. Telling and M. I. Heggie. Radiation defects in graphite. *Philosophical Magazine*, 87:4797, 2007.

[62] Richard Wakeford. The Windscale reactor accident–50 years on. *Journal of Radiological Protection*, 27(3):211, 2007.

[63] Stanley B. Austerman and John E. Hove. Irradiation of Graphite at Liquid Helium Temperatures. *Phys. Rev.*, 100(4):1214–1215, 1955.

[64] H. Jónsson, G. Mills, and K. W. Jacobsen. *Nudged elastic band method for finding minimum energy paths of transitions in Classical and Quantum Dynamics in Condensed Phase Simulations*. World Scientific, Singapore, 1998.

[65] Johannes Kästner and Paul Sherwood. Superlinearly converging dimer method for transition state search. *The Journal of Chemical Physics*, 128(1):014106, 2008.

[66] R. Piessens, E. De Doncker-Kapenga, and C. W. Überhuber. *QUADPACK: a subroutine package for automatic integration*. Springer, 1983.

[67] Oleg A. Vydrov and Troy Van Voorhis. Nonlocal van der Waals Density Functional Made Simple. *Phys. Rev. Lett.*, 103(6):063004, 2009.

[68] T. Thonhauser, Valentino R. Cooper, Shen Li, Aaron Puzder, Per Hyldgaard, and David C. Langreth. Van der Waals density functional: Self-consistent potential and the nature of the van der Waals bond. *Phys. Rev. B*, 76(12):125112, 2007.

[69] William H. Press, Saul A. Teukolsky, William T. Vetterling, and Brian P. Flannery. *Numerical Recipes (3rd edition)*. Cambridge University Press, 2007.

[70] Oleg A. Vydrov and Troy Van Voorhis. Nonlocal van der Waals density functional: The simpler the better. *The Journal of Chemical Physics*, 133(24):244103, 2010.

[71] C. David Sherrill, Tait Takatani, and Edward G. Hohenstein. An Assessment of Theoretical Methods for Nonbonded Interactions: Comparison to Complete Basis Set Limit Coupled-Cluster Potential Energy Curves for the Benzene Dimer, the Methane Dimer, Benzene-Methane, and Benzene-H_2S. *The Journal of Physical Chemistry A*, 113(38):10146–10159, 2009.

This Thesis reflects on efforts towards efficient numerical implementation of the approach and its application to a variety of problems such as molecule adsorption, self-assembly and defects in graphite. Surprisingly for the condensed-matter community, in cases where a molecule is attached to a surface by the "weak" van der Waals forces - they tend to be not so weak after all. These forces can seriously influence kinetics of various physical and chemical processes on surfaces or in layered solids. Hence, ignoring or mishandling the van der Waals interaction potentially leads to quantitatively and sometimes even qualitatively wrong results.

ISBN 978-952-60-4471-2
ISBN 978-952-60-4472-9 (pdf)
ISSN-L 1799-4934
ISSN 1799-4934
ISSN 1799-4942 (pdf)

Aalto University
School of Science
School of Science
www.aalto.fi

BUSINESS + ECONOMY

ART + DESIGN + ARCHITECTURE

SCIENCE + TECHNOLOGY

CROSSOVER

DOCTORAL DISSERTATIONS

Aalto-DD 6/2012

Andris Gulāns

Van der Waals interactions in density-functional theory: implementation and applications

Aalto University